ELSEVIER

Contents lists available at ScienceDirect

# Journal of African Earth Sciences

journal homepage: www.elsevier.com/locate/jafrearsci





# Formation of gold-bearing listvenite in the mantle section of the Neoproterozoic Bir Umq ophiolite, Western Arabian Shield, Saudi Arabia

Hisham A. Gahlan a,b,\*, Mokhles K. Azer , Paul D. Asimow , Khaled M. Al-Kahtany

- a Department of Geology and Geophysics. College of Sciences, King Saud University, Riyadh, 11451, Saudi Arabia
- <sup>b</sup> Geology Department, Faculty of Science, Assiut University, Assiut 71516, Egypt
- <sup>c</sup> Geological Sciences Department, National Research Centre, Cairo, Egypt
- d Division of Geological & Planetary Sciences, California Institute of Technology, Pasadena, CA, 91125, USA
- <sup>e</sup> Seismic Studies Center, College of Science, King Saud University, Riyadh, 11451, Saudi Arabia

#### ARTICLE INFO

#### Keywords: Arabian shield Ophiolite Listvenite Fuchsite Sulphides Gold

#### ABSTRACT

Serpentinized peridotite and associated listvenites of Neoproterozoic age outcrop in the Bir Umq area of western Saudi Arabia. The mantle section of the Bir Umq ophiolite is extensively serpentinized. Serpentinite host samples are low in Al<sub>2</sub>O<sub>3</sub> (0.48-0.75 wt%) and CaO (0.28-1.24 wt%) and have high Mg# (0.90-0.92), indicating a strongly depleted mantle protolith, typically associated with supra-subduction zone environments and more specifically with fore-arc settings. Listvenite bodies of various shapes and sizes developed by alteration of serpentinite. Listvenites occupy the hanging walls of a stack of thrust faults, while serpentinite dominates the footwalls. Based on mineralogical composition and whole-rock geochemistry, the listvenites of Bir Umq are distinguished into carbonate listvenite and silica-carbonate listvenite; the latter is further divided into mineralized and non-mineralized samples. Carbonate listvenite is high in MgO, Fe<sub>2</sub>O<sub>3</sub>, and CaO, but depleted in SiO<sub>2</sub>. Silica-carbonate listvenite is characterized by the presence of rhythmic banding of quartz and carbonate minerals and by the presence of fuchsite. The Bir Umq listvenites preserve various stages of the progressive alteration and metasomatic transformation of their ultramafic protoliths due to interaction with hydrothermal fluids enriched in CO<sub>2</sub>, SiO<sub>2</sub>, Au, K, and other fluid-mobile elements. The association with thrusting suggests that faults acted as conduits for fluids derived from metamorphism of the underlying units during subduction and obduction. Schistosity and deformation fabrics in carbonate listvenite imply that initial listvenitization took place at conditions similar to the conditions of serpentinization. On the other hand, the absence of deformation fabrics in silica-carbonate listvenite suggests that it postdates serpentinization and therefore represents a separate and later fluid infiltration event. Finally, the mineralized silica-carbonate listvenite is highly enriched in fluid-mobile elements Zn, Pb, Cu, Ag, and most notably Au; this enrichment is not correlated with silica content. This suggests that yet a third fluid infiltration event is responsible for the mineralization and Au enrichment. Au concentrations are 0.84-2.31 ng g<sup>-1</sup> in host serpentinite, 26-403 ng g<sup>-1</sup> in carbonate listvenite, 152-545 ng g<sup>-1</sup> in non-mineralized silica-carbonate listvenite, and 2286-3712 ng g<sup>-1</sup> in mineralized silica-carbonate listvenite.

## 1. Introduction

Abundant ophiolites are distinctive components of the Arabian Shield, the eastern part of the Arabian-Nubian Shield (ANS). The ANS is a juvenile tract of continental crust that formed in Neoproterozoic time from a collage of Neoproterozoic juvenile arcs, volcano-sedimentary successions and voluminous granitoid intrusions (e.g., Johnson and Woldehaimanot, 2003; Genna et al., 2002; Meert, 2003; Ali et al., 2010). The ophiolites of the ANS represent fragments of oceanic lithosphere

whose tectonic emplacement onto pre-Pan-African continental margins during closure of the Mozambique ocean caused metamorphism, deformation, cataclasis and mylonitization (Azer and Stern, 2007; Ali et al., 2010; Boskabadi et al., 2017). The Arabian Shield ophiolites are all affected by extensive alteration, marked by chemical changes such as silicification and carbonatization (Ahmed and Hariri, 2008; Gahlan et al., 2020a, b, c; Abuamarah et al., 2020).

Ultramafic members of the ANS ophiolites were transformed by carbonate alteration into distinct lithologies including magnesite, talc-

<sup>\*</sup> Corresponding author. Department of Geology and Geophysics, King Saud University, Riyadh, Saudi Arabia. E-mail address: hjhlan@ksu.edu.sa (H.A. Gahlan).

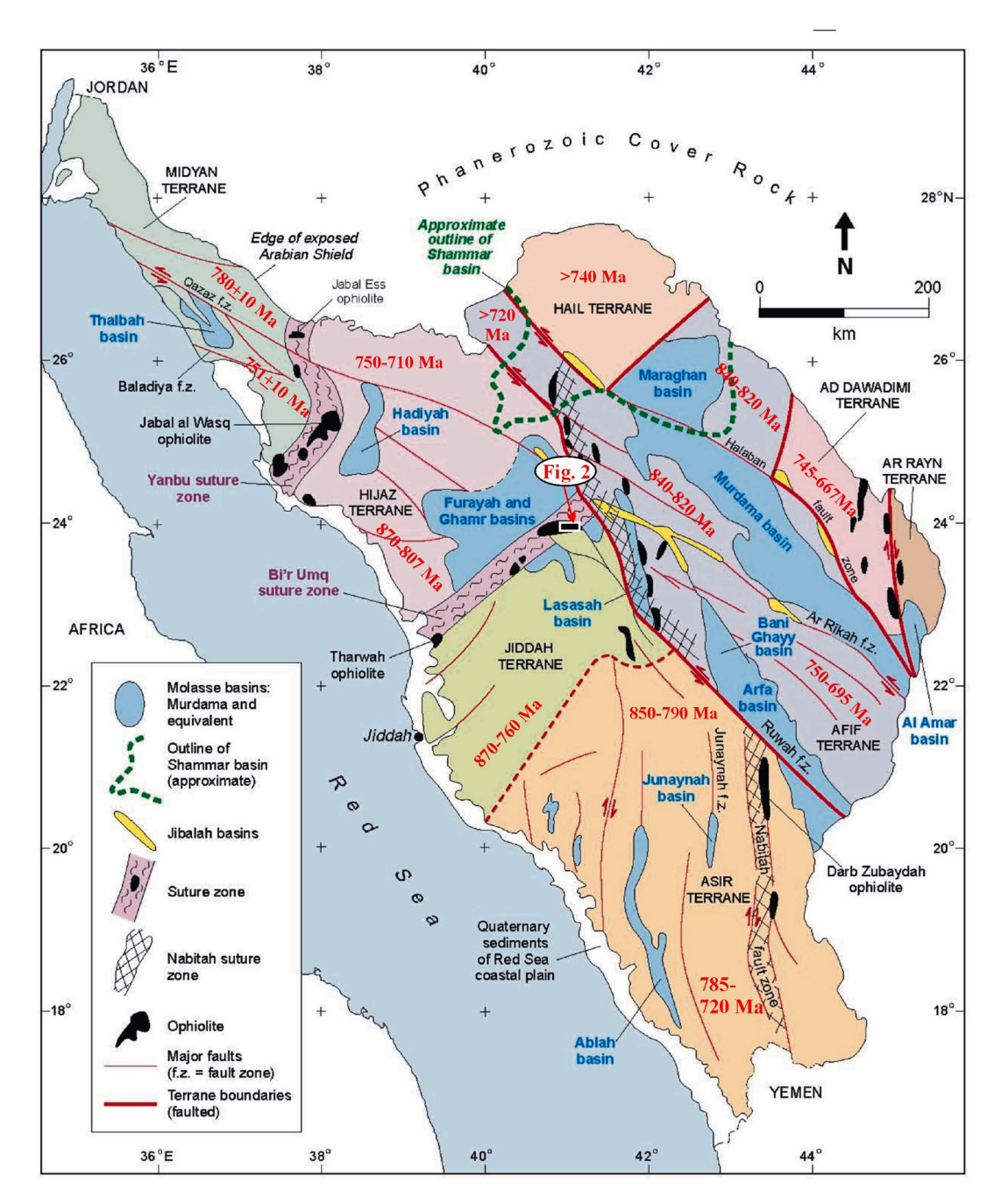


Fig. 1. Regional tectonic map of the Arabian Shield showing the distribution of ophiolitic belts along major suture zones (after Nehlig et al., 2002). The listed ages are from Pallister et al. (1988), Kröner et al. (1991), Agar et al. (1992), Whitehouse et al. (2001) and Hargrove et al. (2006a,b). The study area enlarged in Fig. 2 is noted.

carbonate, and listvenite; mafic layers in proximity to such units may be transformed to rodingite. In this work we focus on listvenite, which refers to an assemblage of carbonate minerals, quartz and Cr-bearing muscovite (fuchsite), together with disseminated sulfides and a variety of accessory minerals (Halls and Zhao, 1995). In the geological literature, a number of spellings of the term "listvenite" have appeared, including "listvanite", "listwanite", and "listwaenite". In the present work, we use the spelling "listvenite," which we judge to be the most correct rendering in English.

Carbonatization of mafic-ultramafic rocks is an important geological process with implications for the formation of ore deposits (Boskabadi et al., 2017; Gahlan et al., 2020a; Moussa et al., 2021) as well as the sequestration of surficial carbon (Power et al., 2013). The

listvenitization of ophiolitic rocks has been a matter of particular interest because of its spatial and temporal association with gold mineralization (e.g., Uçurum, 2000; Akbulut et al., 2006; Pirouei et al., 2020; Gahlan et al., 2020a). A variety of elements are mobilized by the hydrothermal fluids that drive carbonate alteration and may be deposited along with the carbonate. Hence carbonatized and listvenitized shear zones in the mantle section of ANS ophiolites are valuable targets for mineral exploration, particularly for gold (e.g., Zoheir and Lehmann, 2011; Azer, 2013; Gahlan et al., 2018, 2020a; Moussa et al., 2021). Advances in our understanding of listvenite formation and associated mineralization enable refinement of petrogenetic models that support targeted mineral exploration (e.g., Kelemen et al., 2011; Beinlich et al., 2012; Van Noort et al., 2013).

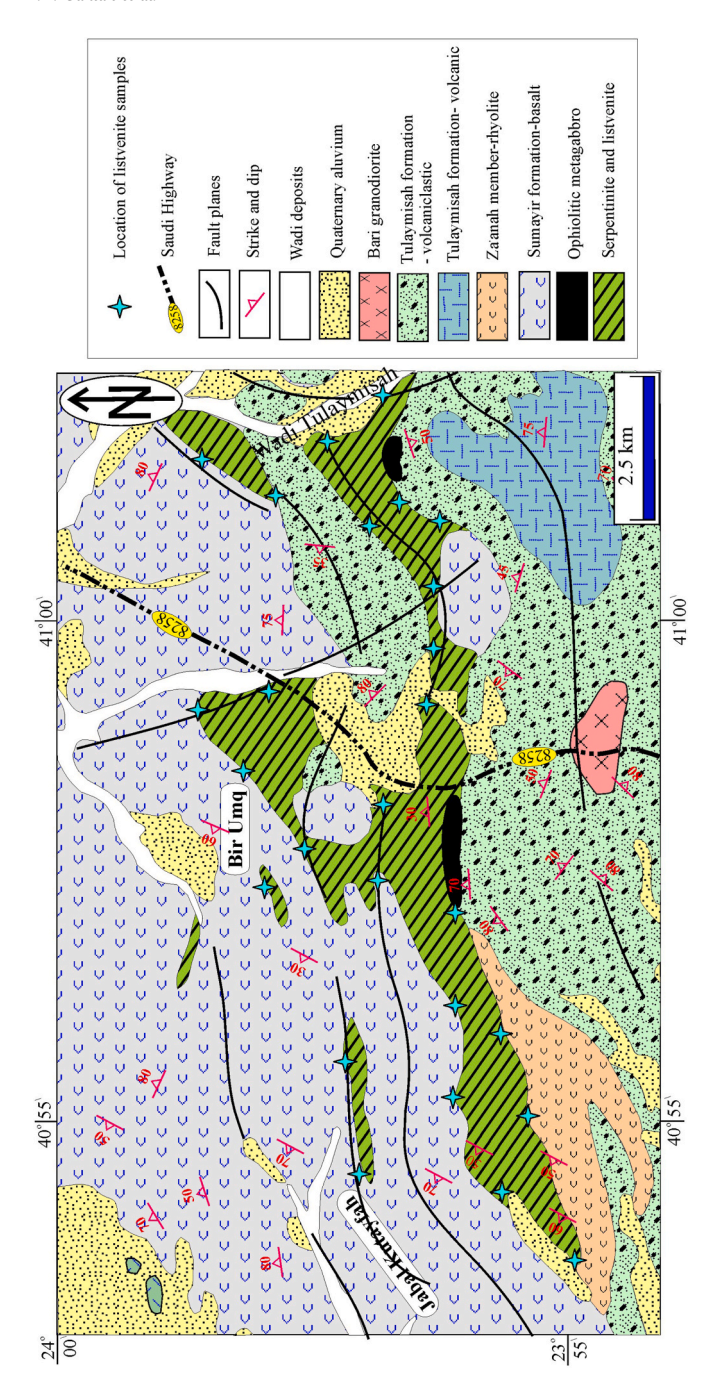


Fig. 2. Geologic map of the Bir Umq area (modified after Kemp et al., 1982).

Although listvenite has long been recognized among the Neoproterozoic rocks of Saudi Arabia, a number of these occurrences have been the subject of renewed study in recent years, motivated primarily by their intimate association with gold mineralization (e.g., Harbi et al., 2003, 2006, 2011; Al Jahdali et al., 2003; 2004; Al Shanti, 2009; Gahlan et al., 2020a). However, the listvenite associated with the Bir Umq ophiolite, despite similarities to other listvenites in Saudi Arabia known to be associated with high gold concentrations, has not been the subject of any recent study. Here we present detailed field work, petrographic study, mineral chemistry, and bulk-rock geochemical data for the Bir Umq listvenites. The chemical analyses of Bir Umq listvenites track the behavior of key chemical elements through progressive stages of alteration and transformation of the primary ultramafic rocks. We apply these data to constrain the sources, compositions and timing of the fluids involved in listvenitization; discuss the assessment of the potential of

listvenites as a source for gold; and propose a basic conceptual model of listvenitization in the area.

## 2. General geology and field observations

The Neoproterozoic Arabian Shield was part of the contiguous ANS before the opening of the Red Sea. It consists of well-defined tectonostratigraphic terranes separated by sutures; these sutures are decorated by a series of ophiolite complexes. A complete, classic ophiolite sequence features a lower "mantle" unit of serpentinized peridotite and an upper "crustal" unit of layered and isotropic gabbro, sheeted dykes, pillow basalts and pelagic sediments. However, most of the Arabian Shield ophiolite sequences are dismembered and lack one or more of their diagnostic lithologies due to folding, shearing and thrusting. Numerous listvenite outcrops have been described in association with the Arabian Shield ophiolites (e.g., Harbi et al., 2003, 2006; Al Jahdali et al., 2003; 2004; Al Shanti, 2009; Abuamarah, 2020; Gahlan et al., 2020a,b), and many of these listvenite occurrences are known to host significant gold enrichment, particularly along shear zones (Al Shanti, 2009; Harbi et al., 2006; Al Jahdali et al., 2003; Al Jahdali, 2004; Gahlan et al., 2020a).

The Bir Umq ophiolite is situated on the western side of Saudi Arabia within an extensive Neoproterozoic fold-and-thrust belt (Fig. 1). The ophiolite outcrops at the northeastern end of the Bir Umq (or Bir Umq-Nakasib) suture, which extends about 600 km in a southwesterly direction across the ANS (Johnson, 2003; Ali et al., 2010). The map area of the Bir Umq ophiolite lies between latitudes  $23^{\circ}$  55′ and  $24^{\circ}$  00′ N and longitudes  $40^{\circ}$  54′ and  $41^{\circ}$  02′ E (Fig. 2). It forms low relief land and is dissected by many strands of the Najd fault system.

The main Neoproterozoic rock units in the Bir Umq area include ophiolitic rocks, volcanic members of an island arc assemblage, and a granodiorite intrusion. Quaternary alluvium and wadi deposits cover some of the Neoproterozoic rock, but basement outcrop makes up >80% of the study area. The ophiolitic rocks occupy an elongated chain of discontinuous hills with an ENE-WSW structural trend. They are thrust between metasedimentary and metavolcanic host rocks. The main unit outcropping north of the serpentinite belt in the study area is the Sumayir formation, which consists mainly of metabasalt with subordinate metatuff and metasedimentary members (Al-Rehaili and Warden, 1980). Some authors have considered the metabasalt and metatuff of the Sumayir Formation to be part of the ophiolite sequence (Al-Rehaili and Warden, 1980; Kemp et al., 1982; Pallister et al., 1988). However, the present field work indicates that the Sumayir Formation is instead part of the island-arc stage volcanosedimentary succession. Along thrust faults and shear zones, the metavolcanic members of the Sumayir formation are carbonatized and have been mapped as listvenite (Al-Rehaili, 1980; Al-Rehaili and Warden, 1980).

The Bir Umq ophiolite is dismembered and consists mainly of serpentinized peridotite with small outcrops of metagabbro, plagiogranite and ophiolitic mélange. A few pockets of metapyroxenite are observed within the metagabbro. The ophiolitic mélange consists of blocks of different sizes and compositions including serpentinite, metabasalt, metadolerite, and metagabbro embedded in a sheared serpentinite matrix. The metagabbro appears out-of-sequence in fault-bounded blocks that are furthermore cross-cut by many vertical faults marked by significant brecciation. In a few outcrops the metagabbro is rodingitized along its margins (Fig. 3a). The ophiolitic metagabbro in this area has yielded a Sm–Nd isochron age of 828  $\pm$  47 Ma (Dunlop et al., 1986). However, plagiogranite intruding the serpentinized peridotite gave zircon model ages of 764–782 Ma (Pallister et al., 1988), which is considered a more robust constraint on the minimum age of ophiolite emplacement.

The Bir Umq ophiolite proper is dominated by serpentinite, much of which is highly fractured and shows a folded schistose foliation indicating extensive shearing (Fig. 3b). The sheared serpentinites are ferruginated due to circulation of fluids along shear planes (Fig. 3c). Along

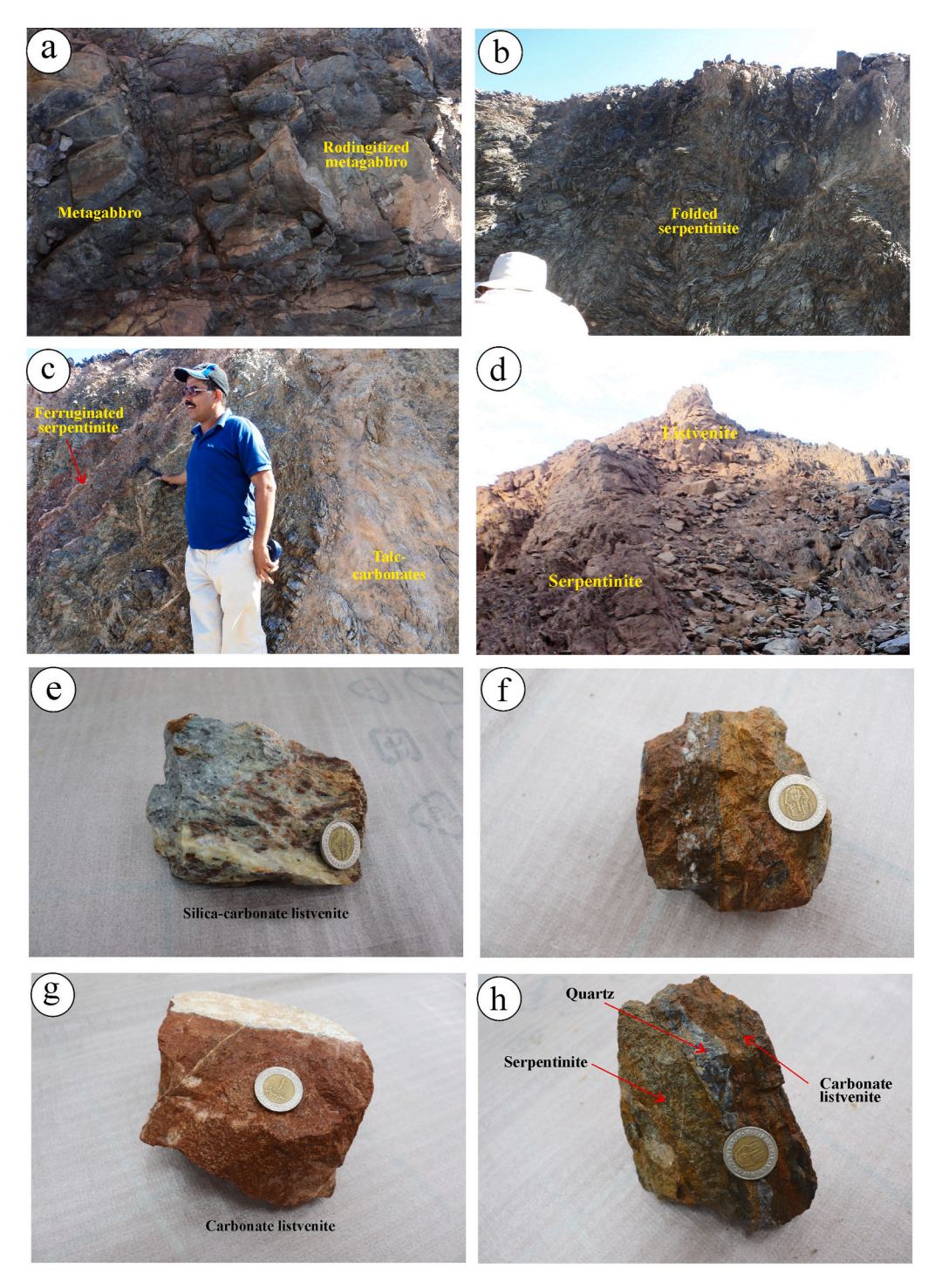
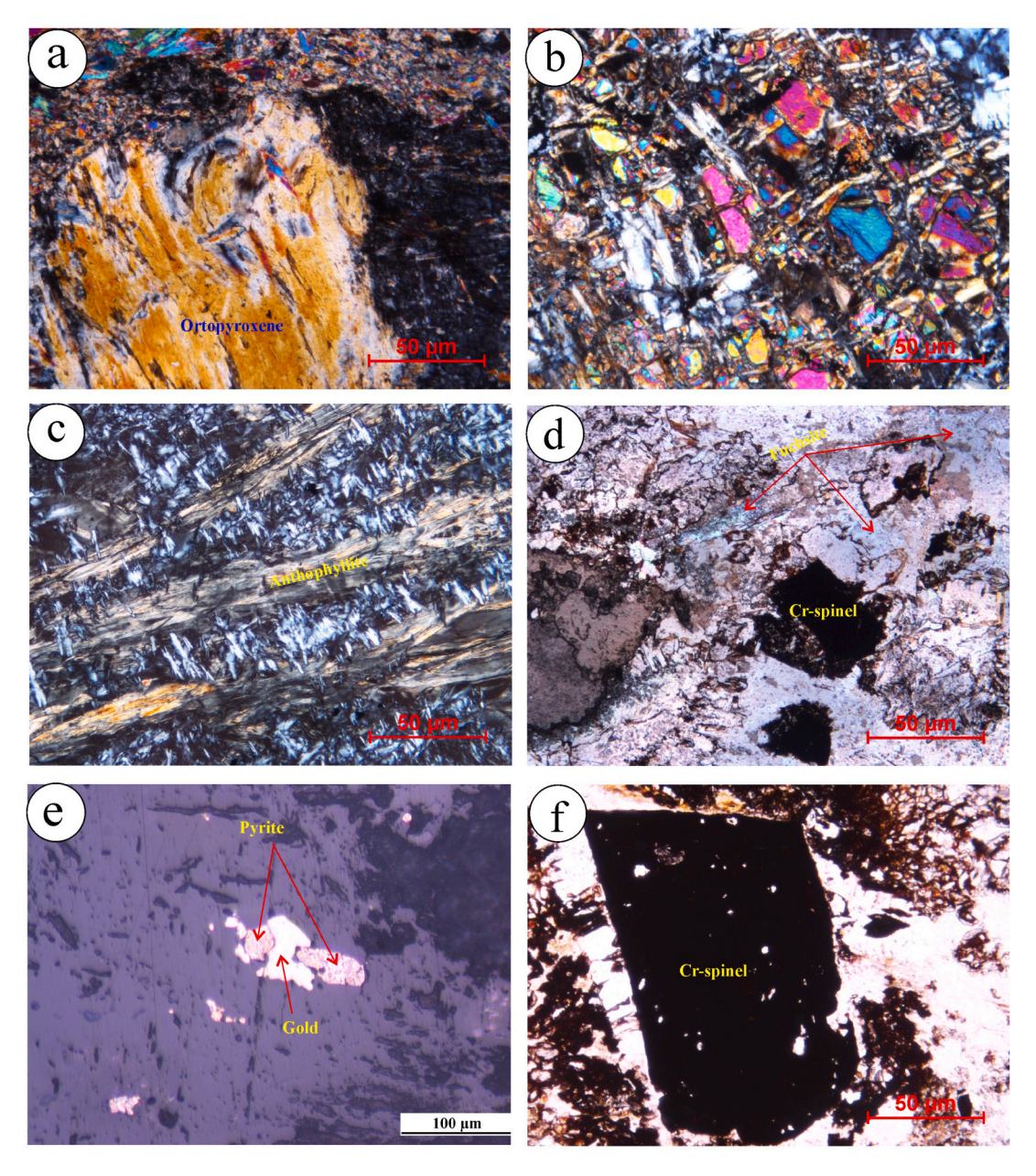


Fig. 3. Field and hand-sample photos of the Bir Umq ophiolite: (a) metagabbro rodingitized along the margins; (b) strongly folded serpentinite; (c) ferruginated serpentinites; (d) ridge of listvenite along a shear zone; (e) greenish grey to reddish grey silica-carbonate listvenite; (f) Rhythmic banding of quartz and carbonates in silica-carbonate listvenite; (g) reddish brown carbonate listvenite; (h) stained carbonate listvenite forming banding with serpentinites and quartz.

shear zones and fault planes, extensive metasomatism and alteration has transformed the ultramafic rocks to talc-carbonates, magnesite and listvenites. A few veinlets and irregular pockets of magnesite and quartz are observed in the sheared serpentinite. The magnesite pockets and veinlets are generally concordant with the serpentinite foliation. The listvenite bodies have a range of different shapes and sizes (Fig. 3d); they are fine-to medium-grained rocks and may appear grey, brownish black, greenish grey, yellowish brown or reddish brown. Some listvenite outcrops show a porous texture. Deformation and schistosity similar to that in the host serpentinite is observed in some listvenite outcrops; small

veins of quartz and carbonates occur in the sheared listvenite bodies.

Based on the field observations, the Bir Umq listvenites are distinguished into two types: carbonate listvenite and silica-carbonate listvenite; the latter is further divided into mineralized and non-mineralized varieties. Silica-carbonate listvenite is more common; it forms upstanding resistant ridges and shows black, grey and green colors (Fig. 3e). Most samples are foliated and rhythmic banding of quartz and carbonate minerals is a characteristic feature (Fig. 3f). Masses of silica-carbonate listvenite may incorporate fragments of serpentinite with gradational contacts. Bright green flecks of fuchsite can be observed in



**Fig. 4.** Photomicrographs showing petrographic textures in serpentinite and listvenites between crossed nicols (a, b and c), plane-polarized transmitted light (d and f) and reflected light (e): (a) fresh relics of orthopyroxene; (b) fresh relics of primary olivine forming interlocking textures; (c) fibers of tremolite in serpentine matrix; (d) fuchsite flakes (light blue); (e) fine speck of gold associated with pyrite; (f) euhedral crystal of Cr-spinel.

hand specimen. Carbonate listvenite is not common and occurs as pockets and lenses of fine-to medium-grained rock. It is yellowish or reddish brown in color (Fig. 3g). A few carbonate listvenite outcrops are stained by iron oxide derived from oxidative weathering of Fe-bearing carbonates (Fig. 3h).

## 3. Petrography

Petrographic studies were carried out on both thin and polished sections of the listvenites and their host serpentinite. The field-based division of listvenite into carbonate and silica-carbonate varieties is confirmed by the petrographic studies. The petrographic characteristics of serpentinized peridotite and associated listvenites are described below.

#### 3.1. Serpentinite

Massive and sheared serpentinite samples have the same mineralogical composition, but in the sheared type the minerals are aligned, defining a schistose foliation. Massive serpentinite is mostly fine-to medium-grained and greenish black. It consists essentially of serpentine minerals with accessory carbonates, tremolite, talc, chlorite and opaque minerals. Serpentine minerals show characteristic mesh and bastite textures indicating alteration of olivine and orthopyroxene, respectively. Primary silicate minerals are rarely preserved as fresh relics, but small rounded crystals of fresh primary orthopyroxene and olivine can be found (Fig. 4a and b).

Antigorite is the essential serpentine mineral, displaying a feather-like habit in massive samples. A few chrysotile veinlets are present, suggesting minor retrograde metamorphism. Sparse cryptocrystalline magnesite occurs as discrete crystals, fine clusters, patches, and fill in through-going fractures. It is stained by reddish-brown by finely

disseminated iron oxide inclusions. The large magnesite crystals show kink banding and fragmentation as well as recrystallization into fine-grained aggregates. Chlorite occurs as fine flakes randomly distributed among the serpentine minerals and carbonates and as rims around altered Cr-spinels, especially ferritchromite. Tremolite and anthophyllite occur as fibrous aggregates embedded in serpentine matrix or as veinlets (Fig. 4c), especially in the serpentinite developed from dunite protoliths.

Opaque minerals include sulfides, magnetite and Cr-spinel. The sulfides include pyrite, chalcopyrite, pyrrhotite and pentlandite. Pyrite occurs mainly as euhedral to subhedral grains randomly scattered among the serpentine minerals. Chalcopyrite occurs as homogenous subhedral to anhedral crystals as well as intergrowths with pyrite. Pyrrhotite is replaced partially or completely by pyrite which, in turn, is oxidized to goethite. Pentlandite is found mainly as small, randomly scattered, anhedral to rounded grains. It is commonly altered to garnierite and Ni-magnetite. Cr-spinel forms deep reddish-brown, euhedral to subhedral crystals that are slightly affected by alteration along grain boundaries and cracks. It is partly replaced by inner rims of ferritchromite and outer rims of Cr-bearing magnetite. Magnetite shows martitization due to oxidation. Scarce gold is observed *in situ* as very fine specks along fractures.

#### 3.2. Silica-carbonate listvenite

Silica-carbonate listvenite samples show a wide range of grain sizes, but medium-grained samples are most common. It consists essentially of quartz and carbonates with accessory talc, chlorite, fuchsite, goethite, illite, vermiculite, fluorapatite, rutile, barite, baddeleyite, and opaque minerals. The modal quartz fraction may be nearly equal to or somewhat greater than that of carbonates. The rhythmic banding of quartz and carbonate minerals is expressed at thin-section scale. Sometimes, the essential minerals show weak preferred orientation and fine magnetite trails define the rock foliation. Late silica and carbonate veinlets are common. Relics of serpentine minerals with mesh texture after olivine are observed in some samples of silica-carbonate listvenite, hinting at their ultramafic protolith.

Quartz forms large anhedral crystals, fine aggregates, and patches. Two stages of silicification are recognized. The first was contemporaneous with carbonatization and led to the formation of microcrystalline quartz, whereas the second stage postdates carbonatization and resulted in coarse quartz crystals corroding the carbonate minerals and filling fractures. The quartz veins cutting silica-carbonate listvenite are brecciated and consist of variously-sized quartz clasts cemented by rhombs of siderite. Fractures in quartz are filled with calcite.

The carbonates are mainly magnesite with minor calcite, dolomite, siderite, and ankerite. Two generations of magnesite are observed. The first generation is often stained with iron oxides. Fine specular hematite decorates the grain boundaries and grains may show polysynthetic twinning outlined by trails of oriented fine magnetite. The second generation is represented by later magnesite veinlets and filled fractures, highly stained by Fe-oxides. Calcite occurs as coarse stained crystals among the magnesite and as veinlet filling. Veinlet calcite includes both equant interlocked crystals and elongated crystals perpendicular to the walls of fractures. Dolomite occurs as zoned rhombs forming bands concordant to the rock foliation. Later siderite rhombs are observed, particularly along silicified fractures.

Fuchsite is observed in some, but not all, samples of silica-carbonate listvenite. It is characterized by its diagnostic green color in plane-polarized light (Fig. 4d) and shows an intimate relationship with highly altered Cr-spinel, often forming a continuous mantle around Cr-spinel relics. Fuchsite also occurs as surface veneers, thin bands, fine green flakes, inclusions in carbonates, and cavity fillings. Talc is formed at the expense of magnesite and occurs as dense aggregates that are occasionally oriented along micro-shear planes. Talc also occurs as large plates and fine aggregates associated with antigorite bundles. Chlorite

occurs as fine flakes squeezed between magnesite and quartz.

Opaque minerals in the silica-carbonate listvenite include Cr-spinel, magnetite, sulfides, nickelphosphide, gold, and patches of Cu mineralization. Cr-spinel is brecciated and occurs as lensoidal crystals altered to ferritchromite at their margins. Rarely, it contains silicate inclusions, altered to chlorite and serpentine. Magnetite occurs as fine, euhedral to anhedral grains interstitial between quartz and carbonates or filling veinlets. Oriented magnetite streaks may trace the original cleavage planes of orthopyroxene in replaced patches of former bastite-textured serpentine. Sulfides are represented by pyrite, pyrrhotite, wurtzite, galena, arsenopyrite, molybdenite, "femolite", and chalcopyrite. Euhedral pyrite grains are mildly oxidized to goethite. Some pyrite crystals are rimmed by later chalcopyrite and others are replaced by arsenopyrite. Pyrrhotite occurs as anhedral to subhedral crystals associated with pyrite or as anhedral specks along fractures. Some pyrrhotite crystals are corroded and replaced by pyrite and others are perfect, homogeneous, six-sided crystals. Very rare and fine composite chalcopyrite-pyrrhotite crystals are observed. Sphalerite occurs as fine disseminated crystals. Nickelphosphide occurs as euhedral and subhedral crystals. Gold occurs as fine specks associated with altered pyrite (Fig. 4e), needle-like crystals and blebs in the quartz veinlets and along fractures in the rock. Also, it occurs as inclusions within large quartz crystals. The patches of Cu mineralization include dioptase, tenorite, and what appears to be a fine aggregate with a (Cu, Fe, Zn)-silicate composition. The identification of accessory minerals, e.g. gold included in goethite, was confirmed by EDS analysis in the SEM (see section 5, Mineral Chemistry).

#### 3.3. Carbonate listvenite

Carbonate listvenite is reddish brown in color due to pervasive staining by Fe oxides. It consists essentially of carbonates (>65 vol%) with smaller amounts of quartz (<30%) and minor talc, chlorite, goethite, baddeleyite, barite, and opaque minerals. Carbonates include mainly magnesite with less calcite, dolomite, and occasional siderite. Magnesite forms granular, optically zoned, lenticular crystals as well as fracture-fill. The coarse magnesite shows a variety of deformation features, ranging from kink to fragmentation and recrystallization into finegrained, highly-stained magnesite aggregates. Rarely, coarse stained magnesite crystals are partly replaced by fine talc flakes. Calcite veinlets are sometimes concordant with rock foliation and are occasionally displaced along micro-faults. Dolomite occurs as late, coarse-grained veins that crosscut the other minerals. Microcrystalline quartz is overgrown and cut by batches and veinlets of magnesite. Chlorite occurs as fine interstitial flakes.

Opaque minerals include Cr-spinel, pyrite, pyrrhotite, chalcopyrite, magnetite, nickelphosphide and gold alloy. Pyrite occurs as subhedral to euhedral crystals; some are visibly sheared. Pyrite is mostly fresh but may be altered along fractures or margins to colloform goethite. The replacement of pyrite by goethite indicates a coupled process of oxidation and hydration. Chalcopyrite occurs as homogenous subhedral to anhedral crystals as well as intergrowths with pyrite, altered in places to covellite. Nickelphosphide is documented in some samples. Cr-spinel is fractured and rarely occurs as euhedral crystals, altered at the margins into ferritchromite and Cr-magnetite (Fig. 4f). Magnetite shows variation in the grain size and slight martitization. Magnetite is strictly confined to the cores of coarse magnesite crystals. Native gold in carbonate listvenite is rare and occurs as fine anhedral crystals.

## 4. Analytical methods

Representative samples of listvenites and associated serpentinite were selected for the preparation of polished thin sections for microprobe analyses. Mineral chemical analyses were performed at the Division of Geological and Planetary Sciences, California Institute of Technology, USA (Caltech) on carbon-coated polished thin sections using a five-spectrometer JEOL JXA-8200 electron microprobe.

Table 1
Major oxides and normative mineralogy in serpentinite of the Bir Umq ophiolite.

Rock type	Serpentir	nized dunite			Serpentir	nized harzbur	gite						
Sample No.	BUD1	BUD2	BUD3	BUD4	BUH1	BUH2	BUH3	BUH4	BUH5	BUH6	BUH7	BUH8	BUH9
Major oxides (v	vt.%)												
$SiO_2$	35.78	36.04	36.6	36.65	38.88	38.53	39.9	39.46	40.58	41.18	38.03	37.04	37.76
TiO <sub>2</sub>	0.02	<d.1.< td=""><td>0.03</td><td>0.04</td><td>0.02</td><td><d.1.< td=""><td>0.03</td><td>0.01</td><td><d.1.< td=""><td>0.02</td><td>0.01</td><td><d.l.< td=""><td>0.02</td></d.l.<></td></d.1.<></td></d.1.<></td></d.1.<>	0.03	0.04	0.02	<d.1.< td=""><td>0.03</td><td>0.01</td><td><d.1.< td=""><td>0.02</td><td>0.01</td><td><d.l.< td=""><td>0.02</td></d.l.<></td></d.1.<></td></d.1.<>	0.03	0.01	<d.1.< td=""><td>0.02</td><td>0.01</td><td><d.l.< td=""><td>0.02</td></d.l.<></td></d.1.<>	0.02	0.01	<d.l.< td=""><td>0.02</td></d.l.<>	0.02
$Al_2O_3$	0.62	0.58	0.52	0.56	0.67	0.64	0.63	0.63	0.71	0.48	0.75	0.68	0.61
$Fe_2O_3^T$	6.88	7.22	7.06	6.74	7.48	6.98	7.98	7.54	7.06	7.3	7.88	7.76	8.1
MnO	0.07	0.09	0.06	0.08	0.08	0.06	0.09	0.07	0.09	0.07	0.07	0.11	0.08
MgO	41.82	42.42	42.67	41.91	38.02	38.07	38.02	37.97	37.57	38.09	38.71	39.42	38.81
CaO	1.16	0.97	0.61	0.89	1.15	1.24	0.47	0.68	0.31	0.28	0.62	0.79	0.77
Na <sub>2</sub> O	0.02	0.02	0.02	0.01	0.01	0.01	0.01	0.01	0.01	0.01	0.01	0.01	0.01
K <sub>2</sub> O	0.02	<d.1.< td=""><td>0.01</td><td>0.01</td><td><d.1.< td=""><td>0.01</td><td>0.02</td><td><d.1.< td=""><td>0.01</td><td>0.01</td><td>0.01</td><td>0.01</td><td>0.01</td></d.1.<></td></d.1.<></td></d.1.<>	0.01	0.01	<d.1.< td=""><td>0.01</td><td>0.02</td><td><d.1.< td=""><td>0.01</td><td>0.01</td><td>0.01</td><td>0.01</td><td>0.01</td></d.1.<></td></d.1.<>	0.01	0.02	<d.1.< td=""><td>0.01</td><td>0.01</td><td>0.01</td><td>0.01</td><td>0.01</td></d.1.<>	0.01	0.01	0.01	0.01	0.01
$P_2O_5$	0.02	0.01	<d.1.< td=""><td>0.02</td><td>0.02</td><td>0.02</td><td>0.02</td><td>0.03</td><td>0.02</td><td>0.01</td><td>0.01</td><td>0.02</td><td><d.l.< td=""></d.l.<></td></d.1.<>	0.02	0.02	0.02	0.02	0.03	0.02	0.01	0.01	0.02	<d.l.< td=""></d.l.<>
LOI	13.29	12.46	12.09	13.15	13.38	14.21	12.68	13.18	13.38	12.24	14.33	14.1	13.43
Total	100.1	99.81	99.67	100.06	99.71	99.77	99.89	99.58	99.74	99.69	100.41	99.94	99.6
CIPW norm													
Orthoclase	_	_	0.07	0.07	_	0.07	0.14	_	0.07	0.07	0.07	0.07	0.07
Albite	-	0.2	0.19	0.1	0.1	0.1	0.1	0.1	0.1	0.1	0.1	0.1	0.1
Anorthite	1.79	1.72	1.49	1.68	2.08	1.97	1.87	1.95	1.64	1.42	2.31	2.09	1.86
Diopside	5.51	2.94	1.56	2.57	3.47	4.01	0.53	1.38	_	0.08	0.95	1.85	2.05
Hypersthene	_	1.88	5.71	7.09	25.01	23.53	32.34	30.5	38.85	39.18	22.27	15.4	19.77
Olivine	90.34	90.96	88.68	86.18	66.91	68.05	62.46	63.63	56.88	56.83	71.81	78.01	73.61
Magnetite	1.76	1.84	1.79	1.73	1.93	1.8	2.04	1.93	1.82	1.85	2.03	2.01	2.09
Hematite	-	_	_	_	_	-	-	_	_	-	_	_	
Ilmenite	0.04	_	0.07	0.09	0.04	-	0.07	0.02	_	0.04	0.02	_	0.04
Apatite	0.05	0.03	_	0.05	0.05	0.05	0.05	0.08	0.05	0.03	0.03	0.05	-
Colour Index	97.65	97.62	97.8	97.66	97.36	97.4	97.44	97.46	97.54	97.98	97.09	97.27	97.56
Diff. Index	-	0.2	0.26	0.17	0.1	0.17	0.23	0.1	0.17	0.17	0.17	0.17	0.17
Mg#	0.92	0.92	0.92	0.92	0.91	0.92	0.90	0.91	0.91	0.91	0.91	0.91	0.90
$MgO/SiO_2$	1.17	1.18	1.17	1.14	0.98	0.99	0.95	0.96	0.93	0.92	1.02	1.06	6

Operating conditions were 15 kV accelerating voltage, 25 nA beam current, a focused beam (1  $\mu$ m), 20 s on-peak counting times, the mean atomic number background subtraction method, a mix of natural and synthetic mineral standards, and the CITZAF matrix correction routine.

Backscattered electron images and energy dispersive X-ray spectra (EDS) were obtained with the Zeiss 1550VP field-emission scanning electron microscope (SEM) in the Division of Geological and Planetary Sciences at Caltech. To detect heavy elements, a 25 kV primary beam was chosen and spectra were collected in the 0–20 kV range. To achieve high spatial resolution and reduce contamination of the spectra of small grains by electron penetration and secondary fluorescence from neighboring phases, the accelerating voltage was reduced for some acquisitions to 15 or 8 kV. Deadtime was maintained below 60% and spectra were integrated for 60 s of live time. The EDS detector is a Si-drift type Oxford Max, and data were processed with Oxford's AZTec software, using factory standards for quantification.

Representative samples of listvenites (20 silica-carbonate listvenite and 7 carbonate listvenite) and serpentinite (13 samples) were analyzed for bulk chemistry (major, trace and REE) at Activation Laboratories Ltd. (Actlabs, Canada). The samples for chemical analyses were crushed in an agate mortar, quartered several times to obtain representative samples, and powdered to ~40 mesh in an agate ring mill. The major oxides were measured by lithium metaborate/tetraborate fusion ICP-AES. Trace and rare earth elements were measured by ICP-MS following lithium borate fusion and acid digestion. In addition, a separate 0.5 g split was digested in hot (95 °C) Aqua Regia and analyzed by ICP-MS to determine precious and base metals. All trace and REE elements concentration are given in  $\mu g g^{-1}$  (parts per million) except that gold is given in  $ng g^{-1}$  (parts per billion). Loss on ignition (LOI) was determined by weight difference after ignition at 1000 °C. Precision and accuracy were controlled by analysis of international reference materials and replicate analyses and are 1% for major elements and 2%-5% for trace elements.

#### 5. Mineral chemistry

The identification of the essential and accessory minerals under the

microscope was refined and supported by microprobe, SEM/EDS and EBSD. However, not all observed essential mineral phases were suitable for microprobe analysis due to the limited number of elements that can be analyzed in a practical protocol and poor totals for carbonates; microprobe data are presented only for arsenic-bearing goethite and for illite. A number of accessory minerals that are too small for quantitative electron probe analysis were identified and analyzed with energy-dispersive X-ray spectroscopy on a high-resolution field-emission SEM. They include gold and gold alloys, sulfides, clay minerals, carbonates, a Ce-rich ZrO<sub>2</sub> phase (possibly baddeleyite), Cu minerals, and barite. Selected backscatter images and EDS spectra of these minerals are reported in Supplementary Fig. 1S to 6S. The complete mineral chemistry dataset is given in the Electronic Appendix (Supplementary Tables A1 to A3).

The most notable features of the mineral chemistry dataset are: (1) the highly elevated concentration of arsenic (average 7.9 wt% and up to 13.1 wt%  $As_2O_3$ ) in goethite in mineralized silica-carbonate listvenite only, (2) the variety of sulfides in silica-carbonate listvenite whether mineralized or not, (3) the confirmed presence of pure Au in mineralized silica-carbonate listvenite versus the presence of Au–Pd–Pt alloy in carbonate listvenite, (4) the unusual Ce- and Zr-rich phase or fine aggregate in both mineralized silica-carbonate listvenite and in carbonate listvenite, and (5) the unidentified (Fe, Cu, Zn)-silicate or fine aggregate in Cu mineralized veins in mineralized silica-carbonate listvenite.

## 6. Geochemistry

## 6.1. Serpentinites

Whole rock geochemical data and the normative compositions of the serpentinized ultramafic samples from the Bir Umq ophiolite are shown in Tables 1 and 2. The analyzed serpentinites have high LOI values (12.1–14.3 wt%), reflecting their near-complete transformation to serpentine (which has  $\sim\!13$  wt% structural  $\rm H_2O$ ). They have SiO $_2$  contents ranging between 35.8 and 41.2 wt% and are high in MgO

Table 2
Trace and REE elements in serpentinite of the Bir Umq ophiolite.

Rock type	Serpentini	zed dunite			Serpentinized harzburgite									
Sample No.	BUD1	BUD2	BUD3	BUD4	BUH1	BUH2	BUH3	BUH4	BUH5	BUH6	BUH7	BUH8	BUH9	
Trace elemen	ts (μg g <sup>-1</sup> )													
Sc	6.22	5.83	6.14	6.38	6.45	7.11	5.22	8.64	6.54	5.85	8.07	6.5	8.36	
Ba	2.76	3.87	2.66	2.33	4.87	5.61	4.54	4.44	4.33	3.66	6.84	4.55	4.47	
Ве	0.86	0.73	0.92	0.49	1.4	0.38	0.42	0.12	0.07	0.14	<d.l.< td=""><td>1.15</td><td>0.7</td></d.l.<>	1.15	0.7	
Ni	2424.66	2818.66	2584.66	2737.33	2343	2279.66	2455	2013.25	2125.33	2055.66	2259.5	2062	2239.66	
Co	107.73	104.96	113.1	108.56	115.2	103.56	118.37	110.32	94.78	94.06	110.07	101.16	102.34	
Cs	0.44	0.59	0.38	0.35	0.32	0.29	0.08	0.12	0.24	0.1	0.17	0.19	0.21	
Ga	1.11	1.26	1.04	1.21	1.05	0.88	1.35	1.15	1.07	0.91	1.08	1.17	1.13	
Hf	0.1	0.14	0.09	0.08	0.08	0.09	0.1	0.06	0.09	0.09	<d.1.< td=""><td>0.2</td><td>0.1</td></d.1.<>	0.2	0.1	
Nb	0.21	0.23	0.19	0.16	0.16	0.1	0.15	0.12	0.13	0.14	0.1	0.15	0.1	
Rb	0.98	1.42	1.03	0.83	1.09	0.79	0.92	0.89	0.77	0.84	0.23	0.37	0.21	
Sn	1.03	1.23	0.92	1.18	0.87	0.24	0.31	0.18	0.14	0.17	0.43	0.53	0.46	
Sr	8.62	6.25	5.98	7.27	12.27	13.04	11.78	10.54	12.39	10.79	11.65	8.35	10.36	
Ta	0.01	0.03	0.01	0.03	0.02	0.02	0.02	0.03	0.02	0.01	0.02	0.02	0.03	
Th	<d.1.< td=""><td>0.05</td><td>0.02</td><td>0.02</td><td>0.05</td><td>0.04</td><td>0.04</td><td>0.05</td><td>0.03</td><td>0.04</td><td>0.04</td><td>0.06</td><td>0.07</td></d.1.<>	0.05	0.02	0.02	0.05	0.04	0.04	0.05	0.03	0.04	0.04	0.06	0.07	
U	0.04	0.02	0.03	0.01	0.06	0.05	0.04	0.04	0.02	0.03	0.06	0.05	0.05	
V	29.96	30.53	32.43	29.76	29.14	30.28	26.55	30.62	27.03	26.6	41.85	32.12	30.96	
W	2.21	2.36	1.71	1.98	0.61	0.43	0.75	0.59	0.68	0.56	2.35	1.75	1.23	
Zr	2.26	1.94	2.06	2.08	2.4	1.96	2.72	2.02	1.92	2.2	2.11	2.17	2.21	
Y	0.46	0.52	0.41	0.35	0.47	0.47	0.32	0.43	0.37	0.38	0.31	0.33	0.3	
Мо	0.13	0.05	0.12	0.14	0.08	0.15	0.14	0.43	0.06	0.14	0.08	0.06	0.21	
Cu	6.08	6.47	6.34	6.43	5.66	6.65	8.61	7.04	4.16	4.73	7.33	4.78	3.96	
Pb	0.37	0.56	0.35	0.48	0.49	0.52	0.49	0.51	0.53	0.47	1.95	0.54	1.25	
Zn	46.81	50.23	46.74	47.88	45.23	42.3	48.45	46.77	45.14	45.16	12.12	19.17	22.08	
	14.48	16.83	9.1	7.96	10.53	8.49	9.46	7.62	9.67	15.15	14.25	14.55	12.53	
As Cd	0.08	<d.l.< td=""><td>0.15</td><td><d.l.< td=""><td><d.l.< td=""><td>0.04</td><td><d.l.< td=""><td><d.l.< td=""><td>0.11</td><td><d.l.< td=""><td>0.12</td><td><d.l.< td=""><td><d.l.< td=""></d.l.<></td></d.l.<></td></d.l.<></td></d.l.<></td></d.l.<></td></d.l.<></td></d.l.<></td></d.l.<>	0.15	<d.l.< td=""><td><d.l.< td=""><td>0.04</td><td><d.l.< td=""><td><d.l.< td=""><td>0.11</td><td><d.l.< td=""><td>0.12</td><td><d.l.< td=""><td><d.l.< td=""></d.l.<></td></d.l.<></td></d.l.<></td></d.l.<></td></d.l.<></td></d.l.<></td></d.l.<>	<d.l.< td=""><td>0.04</td><td><d.l.< td=""><td><d.l.< td=""><td>0.11</td><td><d.l.< td=""><td>0.12</td><td><d.l.< td=""><td><d.l.< td=""></d.l.<></td></d.l.<></td></d.l.<></td></d.l.<></td></d.l.<></td></d.l.<>	0.04	<d.l.< td=""><td><d.l.< td=""><td>0.11</td><td><d.l.< td=""><td>0.12</td><td><d.l.< td=""><td><d.l.< td=""></d.l.<></td></d.l.<></td></d.l.<></td></d.l.<></td></d.l.<>	<d.l.< td=""><td>0.11</td><td><d.l.< td=""><td>0.12</td><td><d.l.< td=""><td><d.l.< td=""></d.l.<></td></d.l.<></td></d.l.<></td></d.l.<>	0.11	<d.l.< td=""><td>0.12</td><td><d.l.< td=""><td><d.l.< td=""></d.l.<></td></d.l.<></td></d.l.<>	0.12	<d.l.< td=""><td><d.l.< td=""></d.l.<></td></d.l.<>	<d.l.< td=""></d.l.<>	
Sb	0.48	0.44	0.13	0.52	0.63	0.53	0.79	0.68	0.11	0.33	0.12	0.49	0.64	
Bi	0.46		0.31	0.32	0.03	0.05		0.08	0.37	0.33	0.44	0.49		
	0.14	0.17	0.11	0.16	0.08	0.05 <d.l.< td=""><td>0.12</td><td>0.15</td><td></td><td>0.11</td><td><d.1.< td=""><td></td><td>0.17 <d.l.< td=""></d.l.<></td></d.1.<></td></d.l.<>	0.12	0.15		0.11	<d.1.< td=""><td></td><td>0.17 <d.l.< td=""></d.l.<></td></d.1.<>		0.17 <d.l.< td=""></d.l.<>	
Ag	0.03	0.04 1.06	0.02	1.01	1.14	<u.i. 0.84</u.i. 	<d.l.< td=""><td>1.32</td><td>0.03</td><td>0.02</td><td>&lt; a.i. 1.27</td><td>0.1 1.56</td><td></td></d.l.<>	1.32	0.03	0.02	< a.i. 1.27	0.1 1.56		
Au (ng g <sup>-1</sup> )	0.99		0.89				2.31	0.05	1.75				0.86	
Hg		0.04		0.07	0.11	0.08	0.12		0.07	0.08	0.06	0.04	0.02	
Se	0.34	0.21	0.22	0.26	0.31	0.25	0.27	0.41	0.38	0.49	0.37	0.44	0.28	
Cr	2660.68	2800.07	2669.52	2946.43	2697.25	2314.43	2203.77	2438.47	2067.72	2032.64	1572.17	1778.07	1318.62	
Li REE (μg g <sup>-1</sup> )	2.36	2.64	2.54	1.96	1.64	3.52	1.43	2.31	4.08	2.83	1.47	2.07	1.67	
La	0.173	0.212	0.229	0.141	0.166	0.178	0.148	0.125	0.166	0.215	0.191	0.107	0.179	
Ce	0.173	0.452	0.518	0.321	0.358	0.178	0.336	0.123	0.353	0.473	0.419	0.107	0.388	
Pr	0.053	0.432	0.065	0.043	0.338	0.412	0.330	0.283	0.333	0.473	0.419	0.240	0.388	
Nd	0.033	0.256	0.003	0.18	0.198	0.032	0.194	0.168	0.205	0.256	0.037	0.054	0.204	
Sm	0.226	0.256	0.279	0.18	0.198	0.221	0.194	0.168	0.205	0.256	0.237	0.154	0.204	
			0.071	0.033	0.049	0.032		0.047			0.009	0.044	0.033	
Eu	0.021	0.024					0.018		0.018	0.022				
Gd	0.061	0.071	0.074	0.063	0.055	0.057	0.056	0.052	0.059	0.069	0.072	0.048	0.053	
Tb	0.011	0.012	0.013	0.011	0.01	0.01	0.01	0.009	0.01	0.011	0.012	0.008	0.009	
Dy	0.066	0.073	0.083	0.074	0.063	0.065	0.068	0.059	0.066	0.079	0.081	0.052	0.062	
Ho	0.014	0.016	0.018	0.015	0.014	0.014	0.015	0.013	0.014	0.017	0.018	0.011	0.014	
Er	0.039	0.045	0.051	0.043	0.039	0.04	0.044	0.038	0.041	0.051	0.053	0.032	0.041	
Tm	0.006	0.007	0.008	0.007	0.006	0.006	0.007	0.006	0.006	0.008	0.008	0.005	0.006	
Yb	0.04	0.046	0.053	0.045	0.041	0.041	0.045	0.041	0.04	0.052	0.053	0.034	0.041	
Lu	0.006	0.007	0.008	0.007	0.006	0.006	0.007	0.006	0.006	0.008	0.008	0.005	0.006	
Eu/Eu*	1.03	1.03	0.97	1.11	1.00	0.90	0.98	1.17	0.98	1.00	0.91	1.13	0.92	
(La/Yb) <sub>N</sub>	2.92	3.12	2.92	2.12	2.74	2.94	2.22	2.06	2.81	2.80	2.44	2.13	2.95	
(La/Sm) <sub>N</sub>	1.71	1.86	2.04	1.68	2.14	2.16	1.67	1.68	1.98	2.06	1.75	1.53	2.13	
(Gd/Lu) <sub>N</sub>	1.25	1.24	1.13	1.10	1.12	1.16	0.98	1.06	1.21	1.06	1.10	1.18	1.08	
(La/Lu) <sub>N</sub>	2.95	3.10	2.93	2.06	2.83	3.04	2.17	2.13	2.83	2.75	2.45	2.19	3.06	

(37.6–42.7 wt%) and Fe<sub>2</sub>O<sub>3</sub> (6.74–8.10 wt%). All the incompatible oxides that are extracted from residual peridotites by melting are low or very low: TiO<sub>2</sub> < 0.03 wt%, Al<sub>2</sub>O<sub>3</sub> < 0.75 wt%, CaO 0.28–1.56 wt%,  $K_2O<0.02$  wt%, and Na<sub>2</sub>O < 0.02 wt%. Using the normative mineralogy, the serpentinized ultramafic rocks are classified as harzburgite and dunite (Fig. 5a). The serpentinized ultramafic samples after harzburgite are richer in SiO<sub>2</sub> ( $\geq$ 38.5 wt%) and lower in MgO ( $\leq$ 38.1 wt%) than those after dunite ( $\leq$ 38.0 wt% SiO<sub>2</sub> and  $\geq$ 38.7 wt% MgO). All serpentinite samples have high Mg# (0.90–0.91, av. 0.91), consistent with oceanic mantle peridotites (Mg# > 0.89; Bonatti and Michael, 1989) and similar to the Mg# of other reported serpentinites in the Arabian Shield (e.g., Gahlan et al., 2020b, 2021, Abuamarah et al., 2020; Moussa et al., 2021). The major element bulk compositions of the serpentinites can be understood as the end-product of partial melt extraction followed by hydration (Fig. 6). We show these relations in

general terms by plotting a polybaric fractional melt extraction trend beginning with the McDonough and Sun (1995) primitive mantle composition and computed using the pMELTS model (Ghiorso et al., 2002). The hydration trend schematically shows the difference between the observed bulk compositions and their anhydrous equivalents.

The trace element contents of the serpentinized ultramafic samples form well-defined patterns, with about 50% relative variability within each lithologic group among elements present at greater than the 1  $\mu g$  g $^{-1}$  level (Table 2). Some of the variability among samples is correlated with major element chemistry and reflects variable magmatic depletion; some variability is analytical, particularly in the very low concentration elements; and some variability likely reflects variable open system redistribution of elements during serpentinization and later alteration. Many trace elements are at or below detection limits in the serpentinite samples. The overall trace element chemistry of each group (i.e.

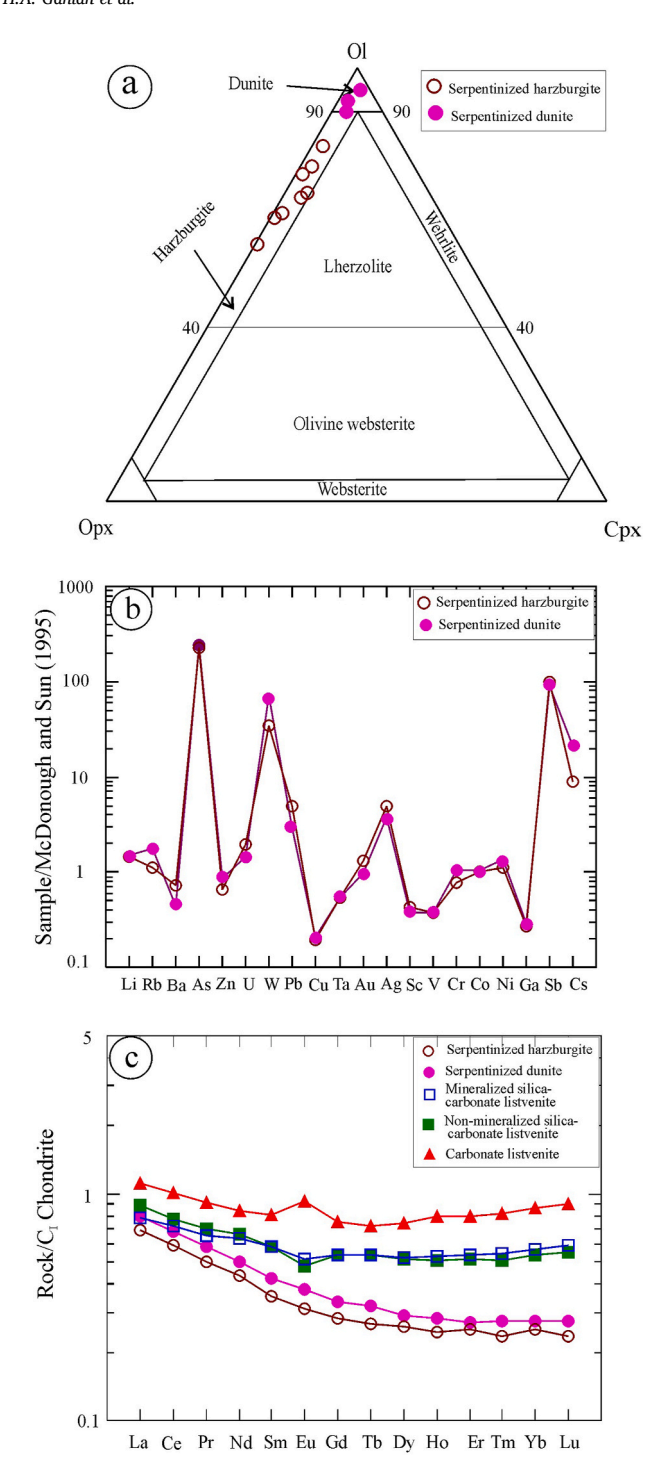


Fig. 5. Whole-rock chemistry plots for serpentinized peridotites: (a) ternary classification diagram for ultramafic rocks (Coleman, 1977), (b) Primitive mantle-normalized trace element patterns for the averages of the Bir Umq serpentinites. Normalization values from McDonough and Sun (1995). (c) Chondrite-normalized rare earth element patterns of the averages of Bir Umq serpentinite and listvenite groups. Chondrite normalization values are from Evensen et al. (1978).

serpentinites after harzburgite and after dunite) is well-represented by plotting the average of each group on a primitive mantle (PM)-normalized trace element diagram (Fig. 5b). At the scale of this diagram, all the individual sample patterns are similar to the averages, and the harzburgite and dunite groups show similar patterns as well. Many trace elements in the serpentinite samples are, perhaps by coincidence, close

to primitive mantle concentrations. There are modest depletions (less than a factor of 5) in Ba, Cu, Sc, V, Ga. The compatible elements Ni (2013–2818  $\mu g \, g^{-1}$ ), Cr (1318–2946  $\mu g \, g^{-1}$ ) and Co (94–118  $\mu g \, g^{-1}$ ) are clustered close to primitive mantle values. Most of the serpentinite samples are enriched to highly enriched in a number of fluid-mobile elements (As, W, Pb, Sb and Cs). There is no significant enrichment in Au (0.84–2.31 ng  $g^{-1}$ ). The trace element patterns do not resemble at all the expectation for a fresh, highly depleted residual peridotite; there is no particular relationship between trace element enrichment or depletion and compatibility during mantle melting. Rather the trace elements reflect comprehensive metasomatism during interaction with fluids that percolated during serpentinization or later alteration events such as carbonatization (Deschamps et al., 2013; Olivier and Boyet, 2006).

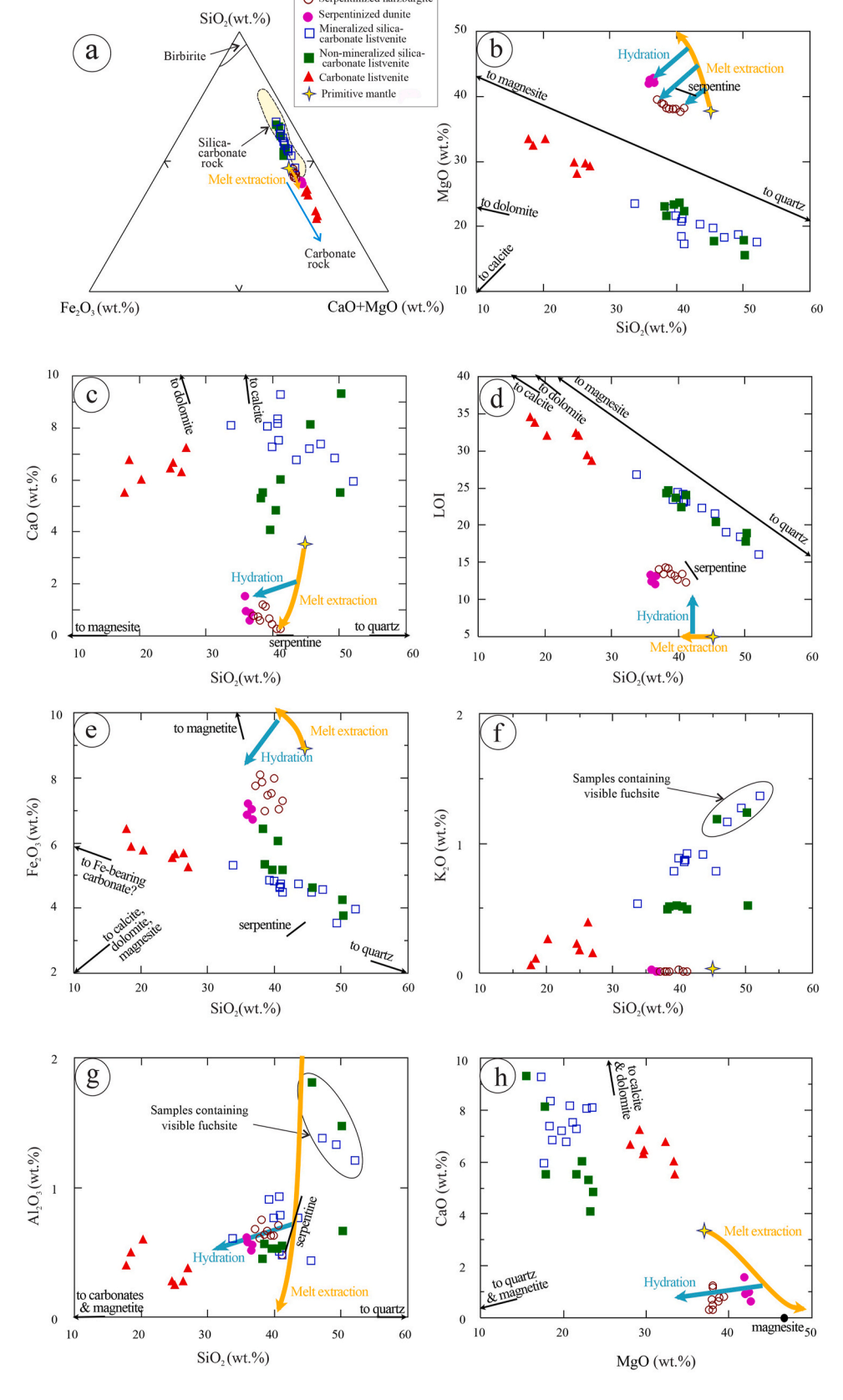
REE concentrations of the serpentinite samples are listed in Table 2. The chondrite-normalized REE patterns for the averages of the two compositional groups of serpentinite samples (i.e., after harzburgite and dunite) are presented in Fig. 5c (using the normalizing values of Evensen et al., 1978). Overall REE concentrations are very low. Total REEs range from 0.80 to 1.49  $\mu g \ g^{-1}$  and CI-normalized concentrations are between 0.2 and 0.9x. The REE patterns in samples from dunite protoliths (SREE = 1.02–1.49  $\mu g \ g^{-1}$ , av. 1.26  $\mu g \ g^{-1}$ ) are parallel to and slightly above those harzburgite protolith samples (0.80–1.39  $\mu g \ g^{-1}$ , av. 1.10  $\mu g \ g^{-1}$ ). The average patterns of both groups are concave-up, with negative slopes indicating modest enrichment of LREE [(La/Lu)\_N = 2.06–3.10] and nearly flat HREE [(Gd/Lu)\_N = 0.98–1.25]. There are no significant anomalies in Eu in serpentinite samples; values of Eu/Eu\* are within analytical error of unity.

As with the broader trace element pattern, the REE patterns do not share any common features with the expected signatures of fresh residual mantle peridotites. Rather the budget of REEs and their patterns are likely controlled by transfer from and exchange with serpentinizing fluids (Paulick et al., 2006; Deschamps et al., 2013). The patterns are similar to a number of serpentinite localities in the Eastern Desert of Egypt (Mubarak et al., 2020) and in Saudi Arabia (Gahlan et al., 2021). The modestly higher REE budget in serpentinized dunite samples may reflect differences in REE compatibility in serpentine with different  $\mathrm{Si/(Mg} + \mathrm{Fe})$  ratio or it may reflect REE uptake in minor secondary mineral phases such as tremolite and anthophyllite. It has been shown, for example, that amphiboles can incorporate significant amounts of REE at hydrothermal temperatures (e.g., Gillis and Meyer, 2001; Boschi et al., 2006).

## 6.2. Listvenites

Twenty-seven representative listvenite samples (7 carbonate listvenite, 8 non-mineralized silica-carbonate listvenite, and 12 mineralized silica-carbonate listvenite samples) were analyzed for major oxides, trace and rare earth elements. The major oxide and trace element concentration data are given in Tables 3-5. As expected from the very different petrographic mineralogy of the listvenite varieties, they differ in major oxide composition, notably in SiO<sub>2</sub>, Fe<sub>2</sub>O<sub>3</sub><sup>T</sup>, CaO, MgO, K<sub>2</sub>O and volatile contents (LOI). The major element whole-rock chemistry of the listvenite samples is shown in Fig. 6, alongside the serpentinite samples. Key end member minerals such as quartz, magnesite, dolomite, calcite, magnetite, and serpentine are indicated where appropriate. A SiO<sub>2</sub>-Fe<sub>2</sub>O<sub>3</sub>-(MgO+CaO) ternary diagram (Fig. 6a) neatly separates the serpentinite and listvenite samples into the groups previously defined on the basis of hand-sample and petrographic observation. Relative to their presumed serpentinite protoliths, carbonate listvenite samples have gained CaO+MgO relative to SiO2, whereas the silica-carbonate listvenite samples (mineralized or not) have gained SiO2 relative to CaO+MgO.

The  $SiO_2$  content of listvenite samples is highly variable. Carbonate listvenite samples have 17.8-26.3 wt%  $SiO_2$ , whereas silica-carbonate listvenite samples have 33.8-52.1 wt%  $SiO_2$ . Although all listvenite samples have lower MgO contents than any serpentinite samples,



O Serpentinized harzburgite

SiO<sub>2</sub>(wt.%)

Fig. 6. Whole-rock major element chemical compositions of the Bir Umq listvenites: (a) SiO<sub>2</sub>–Fe<sub>2</sub>O<sub>3</sub>-(MgO + CaO) ternary diagram. (b) SiO2 vs. MgO. (c) SiO2 vs. CaO. (d) MgO vs. LOI. (e)  $SiO_2$  vs.  $Fe_2O_3$ . (f)  $SiO_2$  vs.  $K_2O$ . (g)  $SiO_2$  vs. Al<sub>2</sub>O<sub>3</sub>. (h) MgO vs. CaO. The primitive mantle composition is from McDonough and Sun (1995); the melt extraction trend is calculated with pMELTS (Ghiorso et al., 2002); typical serpentine compositions are from Deer et al. (1992); other mineral end member shown are pure stoichiometric compositions.

Table 3
Major oxides and trace elements in carbonate listvenite of the Bir Umq ophiolite.

Rock type	Carbonate listve	Carbonate listvenite											
Sample No.	HS2	HS7	HS9	HS11	HS14	HS18	HS25						
Major oxides (wt%)	)												
SiO <sub>2</sub>	25.12	24.64	26.32	27.07	18.53	17.8	20.26						
TiO <sub>2</sub>	0.02	0.01	<d.1.< td=""><td>0.03</td><td>0.01</td><td><d.1.< td=""><td>0.02</td></d.1.<></td></d.1.<>	0.03	0.01	<d.1.< td=""><td>0.02</td></d.1.<>	0.02						
$Al_2O_3$	0.25	0.28	0.28	0.38	0.5	0.4	0.6						
$Fe_2O_3^T$	5.67	5.56	5.7	5.28	5.91	6.44	5.78						
MnO	0.11	0.08	0.11	0.07	0.99	1.12	0.86						
MgO	28.08	29.77	29.69	29.24	32.36	33.42	33.34						
CaO	6.66	6.44	6.3	7.23	6.77	5.52	6.02						
Na <sub>2</sub> O	0.01	0.01	<d.1.< td=""><td>0.01</td><td><d.1.< td=""><td>0.01</td><td><d.1.< td=""></d.1.<></td></d.1.<></td></d.1.<>	0.01	<d.1.< td=""><td>0.01</td><td><d.1.< td=""></d.1.<></td></d.1.<>	0.01	<d.1.< td=""></d.1.<>						
K <sub>2</sub> O	0.17	0.22	0.39	0.15	0.11	0.06	0.26						
$P_2O_5$	<d.1.< td=""><td>0.01</td><td>0.02</td><td>&lt; 0.01</td><td>0.03</td><td><d.l.< td=""><td>0.03</td></d.l.<></td></d.1.<>	0.01	0.02	< 0.01	0.03	<d.l.< td=""><td>0.03</td></d.l.<>	0.03						
LOI	32.11	32.53	29.5	28.68	33.81	34.56	32.05						
Total	98.2	99.55	98.31	98.14	99.02	99.33	99.22						
Trace elements (µg	_												
Sc	4.64	4.17	5.02	5.14	4.08	3.33	4.84						
Ba	32.45	19.55	25.7	26.55	14.44	111.89	17.07						
Ве	1.1	4.94	1.32	1.26	2.06	2.09	2.03						
Ni	1435.11	1534.52	1621.08	1751.51	1381.47	1605.62	1458.07						
Co	77.75	81.74	93.28	83.06	74.87	63.54	86.25						
Cs	0.18	0.14	<d.1.< td=""><td>0.25</td><td>0.43</td><td>0.36</td><td>0.51</td></d.1.<>	0.25	0.43	0.36	0.51						
Ga	0.95	0.56	0.72	0.82	1.43	1.39	1.61						
Hf	0.24	<d.l.< td=""><td>0.15</td><td>0.12</td><td>0.16</td><td>0.12</td><td>0.14</td></d.l.<>	0.15	0.12	0.16	0.12	0.14						
Nb	0.17	0.21	0.11	0.14	0.27	0.24	0.34						
Rb	2.25	1.18	2.24	1.78	4.67	4.27	6.62						
Sn	1.22	0.85	1.09	1.68	1.12	0.93	1.31						
Sr	232.66	227.81	161.68	200.5	145.27	121.66	118.89						
Ta	0.04	0.03	0.02	0.07	0.04	0.07	0.05						
Th	0.12	0.19	<d.1.< td=""><td>0.21</td><td>0.15</td><td>0.06</td><td>0.07</td></d.1.<>	0.21	0.15	0.06	0.07						
U	0.09	0.16	0.12	0.11	0.09	0.05	0.08						
V	22.05	23.14	28.9	21.9	29.32	27.88	31.72						
W	1.25	1.43	1.76	2.28	1.13	0.54	1.73						
Zr	2.15	4.95	2.54	2.98	4.25	5.82	3.77						
Y	0.33	0.45	0.37	0.58	0.62	0.53	0.81						
Mo	0.24	0.17	0.26	0.14	0.22	0.18	0.14						
Cu	31.85	20.77	26.23	21.18	16.85	9.57	16.13						
Pb	7.35	6.85	18.64	16.15	5.87	6.69	13.06						
Zn	51.85	30.4	72.8	40.6	32.15	25.84	39.3						
As	22.4	28.75	45.05	48.3	28.54	30.13	26.89						
Cd	0.26	0.14	0.45	0.22	0.19	0.26	0.31						
Sb	1.55	2.95	1.86	2.75	6.02	3.31	7.73						
Bi	0.17	<d.l.< td=""><td>0.22</td><td><d.l.< td=""><td>0.02</td><td>0.06</td><td>0.12</td></d.l.<></td></d.l.<>	0.22	<d.l.< td=""><td>0.02</td><td>0.06</td><td>0.12</td></d.l.<>	0.02	0.06	0.12						
Ag	0.31	<d.l.< td=""><td>0.22</td><td>0.13</td><td>0.02</td><td>0.04</td><td>0.03</td></d.l.<>	0.22	0.13	0.02	0.04	0.03						
Au (ng g <sup>-1</sup> )	26.13	39.48	402.75	216.25	60.11	119.43	163.62						
Hg (lig g )	0.73	0.67	402.75 0.78	0.46	0.39	0.47	0.54						
Se	0.56	0.45	0.45	0.44	0.38	0.42	0.34						
Cr	1498.81	1476.67	1559.42	1310.14	1602.58	1577.72	1489.43						
Li	9.11	8.14	10.31	12.46	13.58	12.65	14.66						

carbonate listvenite yields higher MgO (28.1–33.4 wt%) than silica-carbonate listvenite (15.6–23.7 wt%) (Fig. 6b). All varieties of listvenite show remarkable enrichment in CaO relative to serpentinite (Fig. 6c), reflecting formation of some calcite in listvenite as opposed to exclusively magnesite in serpentinite. Carbonate listvenite samples yield very high loss on ignition, 28.7–34.6 wt%. LOI in silica-carbonate listvenite samples, though still elevated relative to serpentinite, is notably lower at 16.1-26.8 wt% (Fig. 6d). The carbonate listvenite samples contain total iron content slightly higher than silica-carbonate listvenite, but lower than the serpentinite samples (Fig. 6e), likely reflecting the presence of siderite and ankerite among the carbonates. The silica-carbonate listvenite samples containing visible fuchsite under the microscope have higher contents of  $K_2O$  and  $Al_2O_3$  than the other samples (Fig. 6f and g and Tables 4 and 5).

The compositions of the various listvenite samples form an apparent mixing line in MgO–SiO<sub>2</sub> space between magnesite and quartz components (Fig. 6b), reflecting the dominance of magnesite among the carbonate fraction. This is consistent with the abundance of magnesite in other listvenite occurrences worldwide (e.g., Hinsken et al., 2017). On the other hand, CaO contents are uncorrelated with SiO<sub>2</sub> (Fig. 6c) and only weakly correlated with MgO (Fig. 6h), suggesting a roughly

constant abundance of calcite or dolomite, mostly as late cross-cutting veins, in all listvenite varieties.

The three varieties of listvenite each display a characteristic trace element signature, with variability within each group notably smaller than differences between the groups (Tables 3–5). The carbonate listvenite samples are typically lower in the concentrations of most trace elements, especially fluid-mobile elements, than the silica-carbonate listvenite samples. The silica-carbonate listvenite samples designated as mineralized display extraordinary and well-correlated enrichments in certain elements, notably Zn, Pb, Cu, Ag, As, and Au (Fig. 7a–e). Many of these elements form stable sulfide phases such as arsenopyrite, wurtzite, galena, and chalcopyrite that are often associated with Au and Ag mineralization. In the Bir Umq suite as a whole, Ni correlates with MgO and both concentrations are notably lower in listvenite than in associated serpentinite (Fig. 7f), suggesting that Ni is either removed or diluted during listvenitization of serpentinized ultramafic rocks.

The primitive mantle (PM)-normalized trace elements patterns (normalization values of McDonough and Sun, 1995) for listvenite samples (Fig. 8a) generally show slight to moderate enrichment in large ion lithophile elements (LILE = Rb, Ba, U), and relative depletion in high field strength elements (HFSE, e.g. Ta). The mineralized

Table 4
Major oxides and trace element contents in non-mineralized silica-carbonate listvenite of the Bir Umq ophiolite.

Rock type	Non-mineraliz	Non-mineralized silica-carbonate listvenite											
Sample No.	HS1	HS8	HS10	HS12	HS13	HS19	HS20 <sup>a</sup>	HS21 <sup>a</sup>					
Major oxides (wt	%)												
SiO <sub>2</sub>	50.23	41.11	38.52	39.63	40.45	38.26	45.63	50.05					
$TiO_2$	0.01	0.01	0.01	0.01	0.01	0.01	0.02	0.01					
$Al_2O_3$	0.67	0.55	0.57	0.53	0.53	0.45	1.81	1.48					
Fe <sub>2</sub> O <sub>3</sub> <sup>T</sup>	3.78	5.19	5.35	5.18	6.08	6.45	4.64	4.27					
MnO	0.09	0.09	0.1	0.08	0.09	0.08	0.09	0.12					
MgO	15.59	22.3	21.63	23.29	23.67	23.04	17.76	17.88					
CaO	9.32	6.04	5.51	4.08	4.85	5.29	8.12	5.53					
Na <sub>2</sub> O	0.03	0.03	0.03	0.03	0.03	0.03	0.04	< 0.01					
K <sub>2</sub> O	0.52	0.49	0.51	0.52	0.51	0.49	1.18	1.23					
$P_2O_5$	0.07	0.02	0.02	0.02	0.02	0.02	0.05	0.04					
LOI	18.95	24.12	24.72	23.74	22.44	24.32	20.4	17.75					
Total	99.26	99.95	96.97	97.11	98.68	98.44	99.74	98.36					
Trace elements (µ	ıg g <sup>-1</sup> )												
Sc	4.15	3.98	4.65	5.08	5.28	4.76	3.81	4.69					
Ba	34.62	27.12	37.79	32.62	28.95	25.45	34.11	37.38					
Ве	1.86	2.83	2.64	3.04	1.93	3.05	4.15	3.24					
Ni	1301.11	1464.61	1599.95	1467.45	1475.24	1583.61	1418.18	1393.34					
Co	54.43	75.78	69.18	59.67	71.78	63.8	51.17	62.47					
Cs	0.44	0.43	0.53	0.75	0.56	0.55	1.14	0.54					
Ga	1.75	0.88	1.34	0.99	1.14	0.87	0.97	0.88					
Hf	0.11	0.13	0.14	0.09	0.17	0.14	0.12	0.09					
Nb	0.13	0.06	0.08	0.11	0.08	0.12	0.14	0.09					
Rb	3.36	2.68	3.28	2.78	3.45	2.78	9.31	3.15					
Sn	1.08	0.78	1.02	0.91	1.11	1.05	1.33	0.86					
Sr	115.09	121.89	102.82	99.94	91.99	86.99	108.28	99.89					
Ta	0.08	0.04	0.01	0.05	0.06	0.02	0.04	0.04					
Th	0.08	0.11	0.13	0.09	0.14	0.17	0.07	0.07					
U	0.12	0.08	0.15	0.09	0.21	0.18	0.07	0.02					
v	26.49	31.83	27.83	29.66	30.49	34.16	33.05	38.62					
W	3.46	2.71	2.26	2.41	3.01	1.98	3.84	1.82					
Zr	2.06	2.21	3.98	2.78	2.65	3.11	3.65	3.83					
Y	1.28	0.56	0.53	0.79	0.46	1.03	0.67	0.57					
Mo	0.66	0.35	0.46	0.27	0.31	0.24	0.51	0.42					
Cu	52.09	56.56	44.98	39.44	42.98	37.78	65.61	74.53					
Pb	153.11	127.25	88.81	93.61	119.91	93.6	254.54	222.89					
Zn	125.86	124.36	82.52	86.36	133.69	106.02	139.05	126.08					
As	119.44	123.25	113.67	140.89	126.72	106.89	137.88	95.71					
Cd	0.56	1.27	1.36	0.46	0.67	0.56	0.52	0.29					
Sb	11.89	8.21	10.34	19.99	12.17		13.04	12.17					
Bi	0.08	0.07	0.11	0.12	0.13	13.01 0.09	0.17	0.09					
	0.51	0.41	0.33	0.12	0.13	0.09	0.17	0.09					
Ag (ng g <sup>-1</sup> )	305.05	0.41 226.8	0.33 151.53	0.38 211.08	0.56 307.46	0.41 213.16	0.54 398.75	0.76 545.08					
Au (ng g <sup>-1</sup> )	0.34	0.47	0.41	0.43	0.52	0.37	398.75 0.770	0.78					
Hg			0.41										
Se	1.03 1487.47	1.21		0.83 1969.87	0.95	0.87 2311.92	1.11	1.42 2076.24					
Cr		2103.3	2142.07		2114.78		2466.54						
Li	5.87	6.66	8.09	7.74	7.14	6.98	8.72	6.38					

<sup>&</sup>lt;sup>a</sup> Samples containing visible fuchsite.

silica-carbonate listvenite samples have higher concentrations of LILE and especially of fluid-mobile elements than the other listvenite samples. Au concentrations, in particular, are 26–403 ng g $^{-1}$  in carbonate listvenite, 152–545 ng g $^{-1}$  in non-mineralized silica-carbonate listvenite, and 2286–3712 ng g $^{-1}$  in mineralized silica-carbonate listvenite.

Rare earth element concentrations of listvenite samples are given in Table 6; the carbonate listvenite group stands out as having markedly higher REE abundances ( $\sum$ REE =1.90-2.83; av.  $2.28~\mu g~g^{-1}$ ) than the silica-carbonate listvenite group ( $\sum$ REE =0.56-2.08; av.  $1.64~\mu g~g^{-1}$ ). The averages of the chondrite-normalized REE patterns of each group of listvenite samples are given alongside the average serpentinite REE patterns in Fig. 5c. They show a slight enrichment in LREE relative to HREE [(LaN/Lu)N =1.12-2.02]. The carbonate listvenite group has positive HREE slopes, yielding an overall concave-up pattern. Silica-carbonate listvenite groups show small negative Eu anomalies [(Eu/Eu\*) =0.71-0.98], while the carbonate listvenite group exhibits small positive Eu-anomalies [(Eu/Eu\*) =1.01-1.52].

## 7. Discussion

## 7.1. Alteration and metamorphism

The ultramafic (and mafic) members of the Bir Umq ophiolite sequence are all highly altered and metamorphosed, with mineralogy and trace element signatures completely transformed from those expected in residual peridotites and oceanic basalts. The mantle section experienced penetrative serpentinization, followed by more focused transformation along fault zones and shear planes, yielding carbonate and silica-carbonate listvenite, talc-carbonate rocks, and magnesite. Some of the silica-carbonate listvenite outcrops experienced a third episode of metasomatism, resulting in mineralization and enrichment of fluid-mobile metals to economic grade. Meanwhile, the associated mafic rocks were modified by chloritization and rodingitization. Although the petrographic and geochemical evidence indicates at least three sequential episodes of fluid-driven alteration, aspects of the process remain uncertain. In particular, the absolute timing of the alteration events and the origin, composition, and flux of fluids have all been the subject of some controversy. The conditions of pressure, temperature,

Table 5
Major oxide and trace element contents in mineralized silica-carbonate listvenite of the Bir Umq ophiolite.

Rock type	Mineralize	Mineralized silica-carbonate listvenite												
Sample No.	HS3	HS4	HS5	HS6	HS15*	HS16	HS17	HS22 <sup>a</sup>	HS23	HS24	HS26 <sup>a</sup>	HS27		
Major oxides	(wt%)													
$SiO_2$	40.85	33.77	43.47	40.79	49.19	39.16	39.83	52.08	40.67	45.46	47.14	41.15		
$TiO_2$	<d.l.< td=""><td>0.01</td><td>0.02</td><td>0.03</td><td>0.02</td><td><d.1.< td=""><td>0.01</td><td>0.03</td><td>0.01</td><td><d.1.< td=""><td>0.01</td><td>0.02</td></d.1.<></td></d.1.<></td></d.l.<>	0.01	0.02	0.03	0.02	<d.1.< td=""><td>0.01</td><td>0.03</td><td>0.01</td><td><d.1.< td=""><td>0.01</td><td>0.02</td></d.1.<></td></d.1.<>	0.01	0.03	0.01	<d.1.< td=""><td>0.01</td><td>0.02</td></d.1.<>	0.01	0.02		
$Al_2O_3$	0.79	0.61	0.77	0.51	1.33	0.91	0.77	1.21	0.93	0.44	1.38	0.48		
$Fe_2O_3^T$	4.76	5.32	4.75	4.68	3.56	4.87	4.83	3.98	4.64	4.51	4.57	4.49		
MnO	0.07	0.07	0.41	0.08	0.12	0.08	0.05	0.13	0.08	0.15	0.3	0.19		
MgO	21.19	23.52	20.36	18.53	18.73	22.81	21.63	17.65	20.84	19.78	18.38	17.33		
CaO	7.53	8.09	6.77	8.36	6.86	8.06	7.29	5.94	8.16	7.22	7.38	9.29		
Na <sub>2</sub> O	0.07	0.03	0.06	<d.1.< td=""><td>0.27</td><td>0.11</td><td><d.1.< td=""><td>0.12</td><td>0.08</td><td>0.08</td><td><d.l.< td=""><td>0.05</td></d.l.<></td></d.1.<></td></d.1.<>	0.27	0.11	<d.1.< td=""><td>0.12</td><td>0.08</td><td>0.08</td><td><d.l.< td=""><td>0.05</td></d.l.<></td></d.1.<>	0.12	0.08	0.08	<d.l.< td=""><td>0.05</td></d.l.<>	0.05		
K <sub>2</sub> O	0.87	0.53	0.91	0.85	1.27	0.78	0.88	1.36	0.87	0.78	1.16	0.92		
$P_2O_5$	<d.1.< td=""><td>0.01</td><td>0.03</td><td><d.1.< td=""><td>0.04</td><td>0.02</td><td><d.1.< td=""><td>0.04</td><td>0.03</td><td><d.1.< td=""><td>0.06</td><td>0.02</td></d.1.<></td></d.1.<></td></d.1.<></td></d.1.<>	0.01	0.03	<d.1.< td=""><td>0.04</td><td>0.02</td><td><d.1.< td=""><td>0.04</td><td>0.03</td><td><d.1.< td=""><td>0.06</td><td>0.02</td></d.1.<></td></d.1.<></td></d.1.<>	0.04	0.02	<d.1.< td=""><td>0.04</td><td>0.03</td><td><d.1.< td=""><td>0.06</td><td>0.02</td></d.1.<></td></d.1.<>	0.04	0.03	<d.1.< td=""><td>0.06</td><td>0.02</td></d.1.<>	0.06	0.02		
LOI	23.3	26.79	22.3	24.22	18.48	23.39	24.45	16.11	23.04	21.57	19.05	23.19		
Total	99.43	98.75	99.85	98.05	99.87	100.19	99.74	98.65	99.35	99.99	99.43	97.13		
Trace element	ts (μg g <sup>-1</sup> )													
Sc	4.42	5.14	4.21	9.28	3.98	5.3	4.42	4.15	4.98	3.95	4.49	7.57		
Ba	44.26	40.27	54.08	26.44	66.2	65.06	50.92	79.6	50.13	72.4	27.53	27.87		
Be	3.41	2.52	2.14	3.44	1.88	2.11	2.92	3.07	3.35	2.14	4.85	3.78		
Ni	1538.19	1448.65	1579.38	1445.92	1164.82	1359.81	1402.5	1204.36	1481.51	1334.47	1401.66	1378.61		
Co	65.39	76.09	64.76	92.36	69.37	71.94	66.37	49.88	66.69	64.47	52.95	82.27		
Cs	0.61	0.79	0.48	2.47	0.37	0.98	0.302	0.47	0.89	0.32	0.87	1.13		
Ga	1.21	1.31	1.27	2.37	1.87	1.44	1.26	1.81	1.49	1.22	0.88	1.71		
Hf	0.18	0.24	0.23	1.44	0.16	0.29	0.07	0.14	0.33	0.17	0.12	1.18		
Nb	0.14	0.21	0.07	0.59	0.17	0.18	0.08	0.34	0.12	0.17	0.19	0.47		
Rb	3.16	4.65	2.48	8.77	1.95	5.913	3.87	2.15	7.41	3.85	6.95	12.86		
Sn	0.94	1.73	1.26	2.58	1.75	2.16	0.93	1.68	1.43	1.12	1.29	1.35		
Sr	263.99	270.64	249.48	182.53	252.34	279.52	180.37	172.28	226.78	265.85	96.36	210.77		
Ta	0.03	0.04	0.06	0.08	0.07	0.02	0.07	0.03	0.06	0.04	0.04	0.05		
Th	0.08	0.12	0.09	0.11	0.09	0.13	0.05	0.15	0.08	0.12	0.06	0.05		
U	0.12	0.11	0.14	0.09	0.19	0.14	0.13	0.21	0.12	0.11	0.05	0.08		
v	33.32	29.27	36.38	51.44	24.83	31.37	36.82	41.38	33.56	31.2	36.1	44.51		
w	2.42	2.51	3.51	8.37	3.37	4.14	2.48	2.82	3.45	3.25	3.49	4.75		
Zr	2.43	5.21	2.74	7.36	4.85	5.61	2.22	5.37	2.94	3.65	2.86	5.37		
Y	1.04	0.83	1.13	2.64	2.36	1.61	0.76	2.36	1.48	2.24	0.77	2.14		
Мо	0.34	0.28	0.34	0.47	0.64	0.39	0.32	0.54	0.42	0.71	0.57	0.71		
Cu	99.85	88.34	79.38	106.08	133.59	77.99	62.24	96.12	111.51	101.24	99.66	128.47		
Pb	378.67	306.48	272.63	443.16	549.51	329.93	254.94	364.78	392.13	270.35	333.77	516.62		
Zn	263.04	221.12	233.93	304.26	336.42	176.88	174.05	252.76	294.94	212.45	291.37	383.97		
As	179.45	192.36	184.08	174.45	206.85	155.15	148.33	165.61	223.82	182.73	142.04	250.76		
Cd	0.46	0.39	0.44	0.38	0.52	0.46	0.53	0.43	0.45	0.64	0.61	0.57		
Sb	8.64	8.81	7.61	15.87	9.44	8.74	10.43	7.66	9.14	7.85	12.73	13.85		
Bi	0.15	0.18	0.16	0.21	0.08	0.14	0.12	0.12	0.12	0.16	0.09	0.13		
	1.72	1.38	1.25	1.37	2.11	1.24	1.23	1.48	1.52	1.54	1.64	1.95		
Ag Au (ng g <sup>-1</sup> )	1.72 3283.38	1.38 2864.92	1.25 2856.72	1.37 2979.44	2.11 3689.4	2682.13	2286.48	1.48 2739.15	1.52 3547.75	2718.68	2789.65	3711.56		
	3283.38 0.92	2864.92 0.98				2682.13 0.48						3/11.56 0.49		
Hg	0.92		0.82	1.02 0.92	0.33		1.05	0.45	0.62	0.56	0.64	1.98		
Se		1.14	1.01		0.67	0.89	1.17	0.69	1.26	2.78	1.01			
Cr	1973.51	1871.55	1898.09	2238.63	1732.56	1972.39	2009.44	1592.14	1949.21	1635.47	2252.11	2177.73		
Li	7.93	10.65	6.34	22.2	9.87	13.75	7.3	8.64	10.65	9.11	7.56	13.75		

<sup>&</sup>lt;sup>a</sup> Samples containing visible fuchsite.

and oxygen fugacity prevailing during each alteration episode still require definition as well.

The metamorphic grade implied by the mineral assemblages in the serpentinized ultramafic rocks at Bir Umq range from upper greenschist facies (chrysotile/antigorite-ferritchromite-magnetite) to lower amphibolite facies (talc-tremolite-antigorite-ferritchromite-magnetite). The conditions of initial serpentinization of the ultramafic series are best constrained by the petrographic observation that the dominant serpentine mineral in all the samples is antigorite. Lizardite is very minor and chrysotile is only found in late, cross-cutting veins. Antigorite is most commonly a product of prograde reaction (Deer et al., 1992), forming along a path of increasing pressure and temperature. The abundance of antigorite in Bir Umq serpentinites suggests formation at 400-600 °C during an early high-temperature stage of serpentinization (Evans, 2010). Lizardite, on the other hand, is most commonly a retrograde reaction product, forming along a path of decreasing temperature and pressure. This indicates that the latest episode of serpentinization records an episode of heating and burial (Deer et al., 1992). It is possible that initial retrograde formation of lizardite was overprinted by a second event of prograde recrystallization to antigorite, however the preservation of well-defined

mesh and bastite textures after olivine and orthopyroxene argues against such a two-stage serpentinization (Azer et al., 2019).

Primary Cr-spinel relics are found in all the lithologic varieties of altered ultramafic samples at Bir Umq. In the serpentinized samples, as in the mantle sections of many other ophiolitic occurrences in the ANS (Shahien et al., 2021), Cr-spinel is altered to ferritchromite and Cr-magnetite along cracks and around the crystal boundaries. This is a post-magmatic alteration process that reflects fluid ingress along cracks and through the intergranular medium. The regular structure of these zones, with inner rims of ferritchromite separated by sharp compositional boundaries from outer rims of Cr-magnetite, suggests a two-stage process as opposed to progressively evolving conditions of temperature, fluid composition, and oxygen fugacity (Suita and Strieder, 1996; Barnes and Röeder, 2001; Arai et al., 2006). Alteration of Cr-spinel to ferritchromite is usually attributed to the effects of medium-grade metamorphism (e.g., Thalhammer et al., 1990; McElduff and Stumpfl, 1991) approaching lower amphibolite facies conditions, as the crystal chemistry of nanometric chlorite within ferritchromite indicates minimum temperature of 500 °C (Mellini et al., 2005). The alteration of Cr-spinels to ferritchromite may have started during the late magmatic stage but it

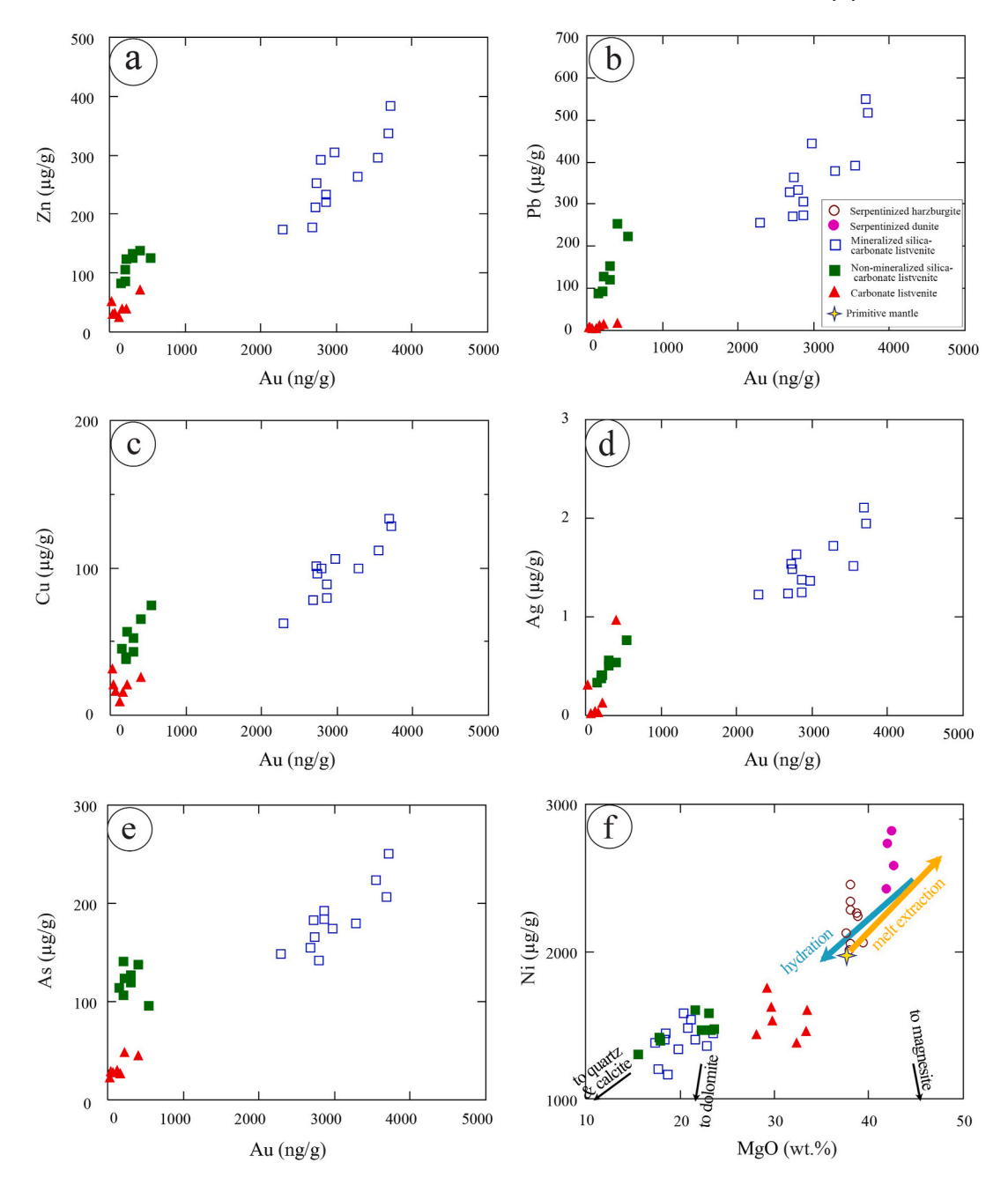


Fig. 7. The variation of Au with other fluid-mobile elements in listvenite samples: (a) Zn, (b) Pb, (c) Cu, (d) Ag and (e) As. (f) MgO (wt. %) vs. Ni ( $\mu$ g g<sup>-1</sup>) in listvenite and serpentinite samples. Primitive mantle composition, melt extraction trajectory, and mineral end members as in Fig. 6.

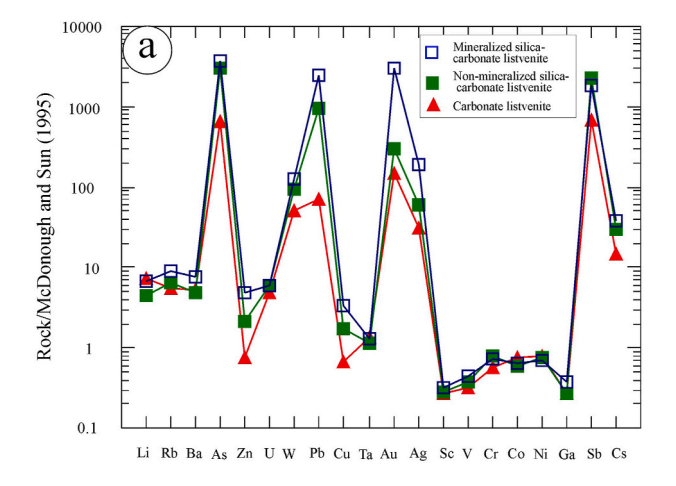
is mainly attributed to the process of serpentinization. The outer Cr-magnetite rims are presumed to indicate a later, lower-temperature, and more oxidizing stage. Note that all the varieties of listvenite contain relics of Cr-spinel with alteration rims resembling those found in the serpentinite samples, suggesting that the Cr-magnetite stage was complete before the onset of carbonation and silicification.

## 7.2. Protolith and geodynamic setting of serpentinites

Studies of the Neoproterozoic ophiolitic rocks of the Arabian Shield initially reached a range of divergent conclusions about their origin and tectonic setting (e.g., Dilek and Ahmed, 2003). These rocks have been assigned by various authors to every oceanic geodynamic setting, including mid-ocean ridge and supra-subduction zone settings (Ahmed et al., 2012; Habtoor et al., 2017). More recently, it has become a clear consensus view that all the Arabian Shield ophiolites formed in

supra-subduction settings (Shahien et al., 2021), and attention has turned to resolving whether they represent back-arc or fore-arc spreading centers. There is considerable support for a fore-arc tectonic setting for all these ophiolites, based on whole-rock chemistry of serpentinite and the compositions of fresh relics of mafic minerals in the mantle sections (Abuamarah et al., 2020; Gahlan et al., 2021).

The Bir Umq serpentinite outcrops are typical of the mantle sections of the Arabian Shield ophiolites and the same arguments about tectonic setting apply. Relict mesh and bastite textures indicate olivine- and orthopyroxene-dominated primary mineralogy. Likewise, whole-rock chemistry reveals normative dunite and harzburgite compositions with high Cr, Ni and Co contents. All the samples of Bir Umq serpentinite have high MgO/SiO $_2$  ratios (0.92–1.18), high Mg#, and low concentrations of TiO $_2$ , Al $_2$ O $_3$  and CaO. All these are features of highly refractory mantle material (Deschamps et al., 2013) residual to high degrees of partial melt extraction. These features are diagnostic of oceanic peridotites



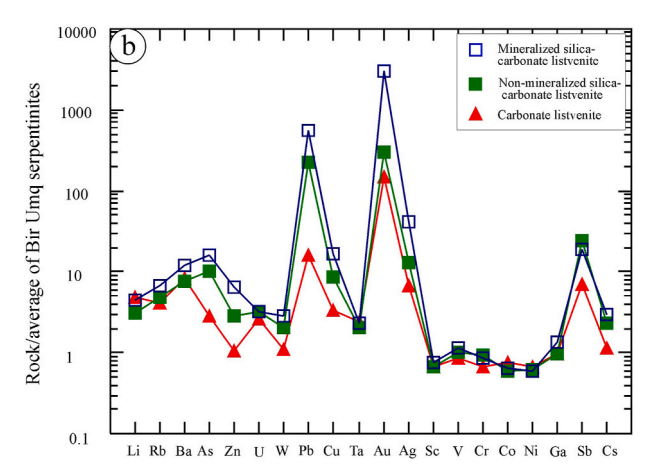


**Fig. 8.** (a) Primitive mantle-normalized trace elements patterns for the averages of the listvenite sample groups. Normalization values are after McDonough and Sun (1995). (b) Spider diagram for the averages of each listvenite group normalized to the average of the associated serpentinite.

(Mg# >0.89; Bonatti and Michael, 1989) and more specifically of fore-arc supra-subduction zone peridotites (e.g., Deschamps et al., 2013; Salters and Stracke, 2004). On the MgO/SiO2 vs. Al2O3/SiO2 diagram (Jagoutz et al., 1979; Hart and Zindler, 1986), the serpentinite samples after harzburgite plot at low Al<sub>2</sub>O<sub>3</sub>/SiO<sub>2</sub> (Fig. 9a) in the area of overlap between the most depleted abyssal peridotites and typical fore-arc peridotites. However, in the Al<sub>2</sub>O<sub>3</sub> vs. CaO plot, the serpentinite samples after harzburgite plot beyond the most depleted abyssal peridotites and in a position more consistent with fore-arc affinity (Fig. 9b). The samples after dunite were likely affected by melt-rock reaction processes that moved them off the main melt depletion trend (Kelemen et al., 1997). The most recent overall model for the evolution of the Egyptian ophiolites in a fore-arc suprasubduction zone (Azer and Stern, 2007; Azer and Asimow, 2021) was proposed by Abdel-Karim et al. (2021). This model sets the several stages required to generate the ANS ophiolites in the context of the opening and subsequent closing of the Mozambique Ocean between East and West Gondwana (Fig. 10).

## 7.3. Petrogenesis of listvenite rocks

Listvenite is the product of metasomatic alteration of ultramafic protoliths by processes such as carbonation, silicification and potassic alteration. During such processes, primary mafic silicate minerals are replaced by an assemblage of quartz, carbonates and chromian micas (Buisson and Leblanc, 1987; Halls and Zhao, 1995; Uçurum, 2000; Plissart et al., 2009; Azer, 2013; Gahlan et al., 2018, 2020a). Here we discuss the details of these processes recorded in the Bir Umq listvenites

and discuss the implications for mineral potential and for related list-venite occurrences elsewhere in the ANS and worldwide.

Although the listvenite bodies in the Bir Umq area have various shapes and sizes, they are all closely associated with zones of focused shear, deformation, and fault displacement. The whole rock geochemical data confirm the petrographic observation that listvenitization of serpentinite is accompanied by extensive metasomatic modification of both major and trace element contents of the affected samples. Nevertheless, the ultramafic nature of the protoliths of the listvenites is confirmed by the presence of relict Cr-spinel and elevated whole-rock Cr, Co and Ni contents. The most notable chemical changes are addition of CO<sub>2</sub> and SiO<sub>2</sub>, but most other elements are affected to some degree. The original field-based division of listvenite outcrops into carbonate listvenite and silica-carbonate listvenite proves useful for understanding the range of chemical changes that fall into the broad category of listvenitization processes (Figs. 6–8).

The hydrothermal fluids that drive alteration of serpentinite and support metasomatic chemical changes leading to listvenite by exchanging solutes with the protoliths have been variously attributed to: 1) CO<sub>2</sub>-rich fluids derived from mantle sources (e.g., Newton and Stern, 1990; Lebda, 1995; Boskabadi et al., 2017; Hamdy and Gamal El Dien, 2017), 2) metamorphic and meteoric hydrothermal fluids (e.g., Likhoidov et al., 2007; Hamdy and Lebda, 2007), and 3) mixing of these two sources (Gahlan et al., 2018). Given the evidence from Bir Umq of three distinct varieties of listvenite, we can reconcile these views by invoking at least three successive episodes of fluid infiltration, with different fluid sources and compositions. Similar multistage histories have been proposed for other listvenite localities in the ANS (Gahlan et al., 2018, 2020a). For reasons we discuss below, a progressive evolution of the fluid composition during a single episode of alteration does not explain the combination of chemical and structural data from Bir Umq.

We infer that the first stage of listvenitization led to the development of carbonate listvenite and that this stage was contemporaneous with serpentinization. In the fore-arc setting where the Bir Umq ophiolite was emplaced, the source of  $\mathrm{CO}_2$  at this stage was probably decomposition of subducted, carbonate-bearing sedimentary rocks delivered to the underlying accretionary prism by oceanic subduction (Azer et al., 2019). This source can yield a larger and more focused flux of  $\mathrm{CO}_2$  than general, non-slab-derived mantle fluid. The carbonate minerals in the carbonate listvenite preserve evidence of deformation by high-temperature plastic strain in the form of kink banding and grain-size reduction. The serpentinites preserve evidence of similar deformation, supporting a common high-temperature history of serpentine and carbonate minerals in the sequence.

We then infer that the development of silica-carbonate listvenite preserves a second stage of listvenitization. Silica-carbonate listvenite may form directly from serpentinite or by further alteration of carbonate listvenite. The absence of deformation fabrics in the silica-carbonate listvenite suggests that they post-date serpentinization and represent modification after cooling below the temperatures of plastic deformation. Thus, the source of silica is unlikely to be the local conversion of serpentinite to carbonate during carbonate listvenite formation. Rather, the association with brittle faults indicates fluid infiltration along lowtemperature localized deformation zones, probably contemporaneous with the obduction of the ophiolite along thrust planes. At this stage, the source of metasomatic, SiO2-saturated and CO2-bearing, fluids is the footwall of the obduction thrust structure. Rocks in the footwall likely include continental-shelf facies clastic and carbonate sediments with abundant pore fluid rich in silica and CO2. The alteration of Cr-spinel to form ferritchromite and Cr-magnetite in both serpentinites and silicacarbonate listvenite indicates that these fluids were highly oxidizing. The presence of Cr-muscovite (fuchsite) in the silica-carbonate listvenites indicates that at least some of the fluid at this stage was rich in K. Similarly, the presence of barite and the ~10-fold enrichment in Ba in listvenite compared to serpentinite reveals that the fluid was enriched in Ba as well.

**Table 6** REE contents ( $\mu g g^{-1}$ ) in listvenites of the Bir Umq ophiolite.

Rock type	Carbonate listvenite	Non-mi	neralized s	ilica-carbo	nate listve	enite									_
Sample	HS2	HS7	HS9	HS11	HS14	HS18	HS25	HS1	HS8	HS10	HS12	HS13	HS19	HS20 <sup>a</sup>	HS21 <sup>a</sup>
La	0.348	0.283	0.274	0.223	0.242	0.261	0.253	0.248	0.221	< 0.1	0.264	0.201	0.151	0.187	0.197
Ce	0.761	0.652	0.702	0.491	0.539	0.579	0.579	0.551	0.467	0.298	0.547	0.463	0.368	0.448	0.483
Pr	0.104	0.091	0.101	0.071	0.077	0.082	0.084	0.076	0.065	0.052	0.081	0.067	0.051	0.062	0.065
Nd	0.475	0.394	0.434	0.336	0.352	0.382	0.378	0.354	0.315	0.262	0.365	0.31	0.248	0.289	0.296
Sm	0.156	0.125	0.132	0.103	0.109	0.126	0.115	0.108	0.097	< 0.05	0.111	0.092	0.064	0.082	0.076
Eu	0.085	0.067	0.05	0.053	0.043	0.048	0.043	0.038	0.026	< 0.02	0.029	0.032	0.022	0.025	0.021
Gd	0.187	0.163	0.174	0.13	0.137	0.146	0.143	0.133	0.13	< 0.05	0.126	0.113	0.074	0.1	0.091
Tb	0.032	0.029	0.03	0.024	0.025	0.026	0.026	0.024	0.025	< 0.01	0.024	0.02	0.013	0.017	0.015
Dy	0.225	0.208	0.196	0.165	0.175	0.186	0.178	0.156	0.152	< 0.05	0.176	0.136	0.083	0.115	0.101
Но	0.054	0.048	0.045	0.037	0.039	0.043	0.049	0.035	0.032	0.014	0.041	0.029	0.019	0.029	0.021
Er	0.167	0.141	0.135	0.109	0.115	0.134	0.123	0.104	0.086	0.052	0.127	0.084	0.053	0.076	0.064
Tm	0.026	0.023	0.022	0.017	0.018	0.021	0.021	0.016	0.013	0.014	0.021	0.013	0.008	0.013	0.01
Yb	0.181	0.159	0.151	0.121	0.128	0.149	0.138	0.11	0.091	0.052	0.142	0.089	0.052	0.084	0.066
Lu	0.031	0.026	0.024	0.018	0.019	0.023	0.021	0.018	0.013	< 0.01	0.021	0.013	0.008	0.013	0.01
Eu/Eu*	1.52	1.43	1.01	1.40	1.08	1.08	1.02	0.97	0.71	-	0.75	0.96	0.98	0.84	0.77
(La/Yb) <sub>N</sub>	1.30	1.20	1.23	1.25	1.28	1.18	1.24	1.52	1.64	-	1.26	1.53	1.96	1.51	2.02
$(La/Sm)_N$	1.41	1.43	1.31	1.37	1.40	1.31	1.39	1.45	1.44	-	1.50	1.38	1.49	1.44	1.64
(Gd/Lu) <sub>N</sub>	0.74	0.77	0.89	0.89	0.88	0.78	0.83	0.91	1.23	-	0.74	1.07	1.13	0.94	1.12
(La/Lu) <sub>N</sub>	1.15	1.12	1.17	1.27	1.31	1.16	1.23	1.41	1.74	-	1.29	1.58	1.93	1.47	2.02

Rock type	Mineraliz	ed silica-carbo	onate listvenit	e								
Sample No.	HS3	HS4	HS5	HS6	HS15*	HS16	HS17	HS22*	HS23	HS24	HS26 <sup>a</sup>	HS27
La	0.135	0.211	0.201	0.189	<0.1	0.188	0.196	0.235	0.201	0.162	< 0.1	0.199
Ce	0.339	0.52	0.499	0.449	0.225	0.425	0.368	0.529	0.43	0.395	0.191	0.467
Pr	0.044	0.071	0.071	0.064	< 0.02	0.06	0.053	0.075	0.062	0.053	< 0.02	0.064
Nd	0.217	0.321	0.328	0.305	0.29	0.306	0.278	0.343	0.307	0.254	0.201	0.303
Sm	0.062	0.09	0.097	0.089	< 0.05	0.098	0.088	0.102	0.095	0.074	0.078	0.09
Eu	0.019	0.031	0.031	0.032	< 0.02	0.031	0.024	0.035	0.032	0.021	0.025	0.03
Gd	0.075	0.112	0.125	0.113	< 0.05	0.12	0.117	0.121	0.125	0.091	0.082	0.107
Tb	0.012	0.019	0.022	0.02	< 0.01	0.021	0.021	0.022	0.023	0.016	< 0.01	0.019
Dy	0.074	0.134	0.146	0.138	< 0.05	0.141	0.151	0.153	0.157	0.11	0.078	0.129
Но	0.017	0.03	0.033	0.031	0.042	0.029	0.035	0.035	0.035	0.024	0.037	0.029
Er	0.047	0.088	0.099	0.092	< 0.03	0.077	0.104	0.106	0.109	0.074	0.057	0.089
Tm	0.008	0.014	0.016	0.014	< 0.01	0.012	0.016	0.017	0.017	0.011	0.046	0.014
Yb	0.056	0.095	0.109	0.101	< 0.05	0.08	0.116	0.116	0.124	0.074	0.057	0.094
Lu	0.009	0.015	0.017	0.015	< 0.01	0.012	0.017	0.018	0.018	0.011	< 0.01	0.014
Eu/Eu*	0.85	0.94	0.86	0.98	_	0.87	0.72	0.96	0.90	0.78	0.96	0.93
(La/Yb) <sub>N</sub>	1.63	1.50	1.25	1.27	_	1.59	1.14	1.37	1.10	1.48	-	1.43
(La/Sm) <sub>N</sub>	1.37	1.48	1.31	1.34	-	1.21	1.41	1.45	1.34	1.38	_	1.40
(Gd/Lu) <sub>N</sub>	1.02	0.92	0.90	0.92	_	1.23	0.84	0.82	0.85	1.01	-	0.94
(La/Lu) <sub>N</sub>	1.54	1.44	1.21	1.29	-	1.61	1.18	1.34	1.14	1.51	-	1.46

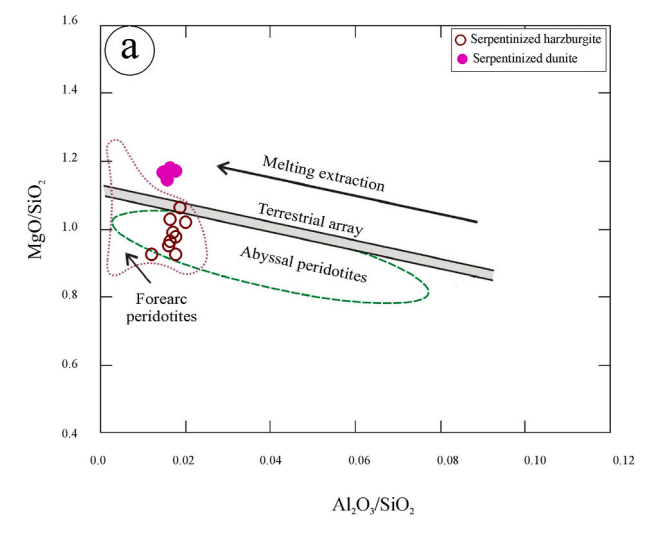
<sup>&</sup>lt;sup>a</sup> Samples containing visible fuchsite.

Finally, the Bir Umq listvenites have variable contents of fluidmobile elements (As, Sb, Sr, Ag, Pb, and especially Au) extending to enrichment of nearly 1000-fold. We recognize a sub-category of mineralized silica-carbonate listvenites that have been particularly affected by addition of fluid-mobile elements and the growth of associated ore minerals. The enrichment in fluid mobile elements is not correlated with increase in silica content and so these samples do not simply represent more extensive reaction with the silicifying fluid. Instead, the mineralized silica-carbonate listvenites likely represent yet another episode of fluid infiltration, possibly derived from magmatic fluids from nearby or subjacent felsic intrusions (e.g., the Bari granodiorite). The low temperature of the listvenite bodies in the hanging walls of shallow thrust faults at this stage promoted precipitation of transported elements as sulfides, Cu minerals, goethite, and native gold. The observation that mineralization and Au-enrichment is found only in the silica-carbonate listvenites likely indicates reactivation of the fluid pathways developed during silicification as preferred conduits for the late mineralizing fluid.

Given the evidence that the listvenites at Bir Umq formed by replacement of serpentinite, we assess the relative mobility of each major oxide and trace element by comparing the average concentrations in each listvenite group to the average concentrations in all the serpentinite samples (the differences among serpentinites are minor by comparison). All the listvenite varieties are enriched in CaO,  $Na_2O$  and

K<sub>2</sub>O, but depleted in MgO. The gains and losses of the trace elements during the alteration of serpentinites to listvenites are shown in Fig. 8b, where the average trace element abundances of the listvenite groups are normalized to the average abundance in the associated serpentinites. The listvenite groups display relative enrichment in Li, Rb, Ba, As, Zn, U, W, Pb, Co, Ta, Au, Ag, Sb and Cs. The most notable gains are in Pb, Au, Ag, and Sb. Although As is extremely enriched in listvenite, it is also highly enriched in serpentinite, and so the relative enrichment does not stand out as extraordinary (about one order of magnitude in silicacarbonate listvenite). Some other elements are nearly equal in listvenites and serpentinite (Sc, V, Cr, Co, Ni and Ga). The pattern of enrichment in REE in the listvenite groups relative to the serpentinite groups is apparent in Fig. 5c: there is slight enrichment in LREE (10-20% in silicate-carbonate listvenite and 50% in carbonate listvenite) but significant enrichment in HREE (~200% in silicate-carbonate listvenite and >300% in carbonate listvenite). In most fluid-mobile trace elements, the carbonate listvenite average is least enriched, the nonmineralized silica-carbonate listvenite average is intermediate, and the mineralized silica-carbonate listvenite average is most enriched. However, the compatibility of REE in carbonates yields the opposite pattern, with carbonate listvenite being more enriched in REE than silicatecarbonate samples.

The current results are comparable to other studies specifically within the Eastern Desert of Egypt (Ramadan et al., 2005; Zoheir, 2011;



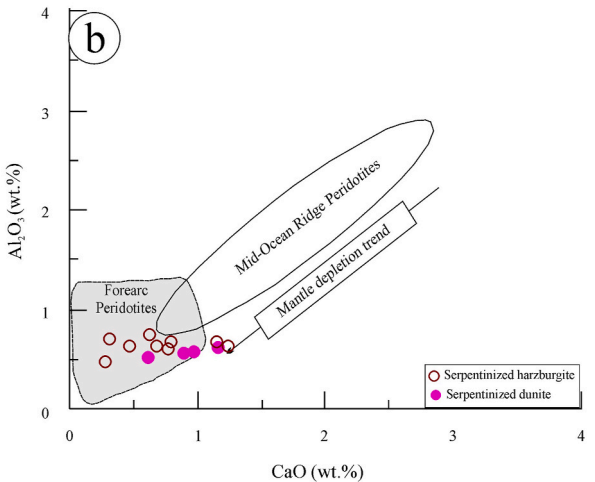
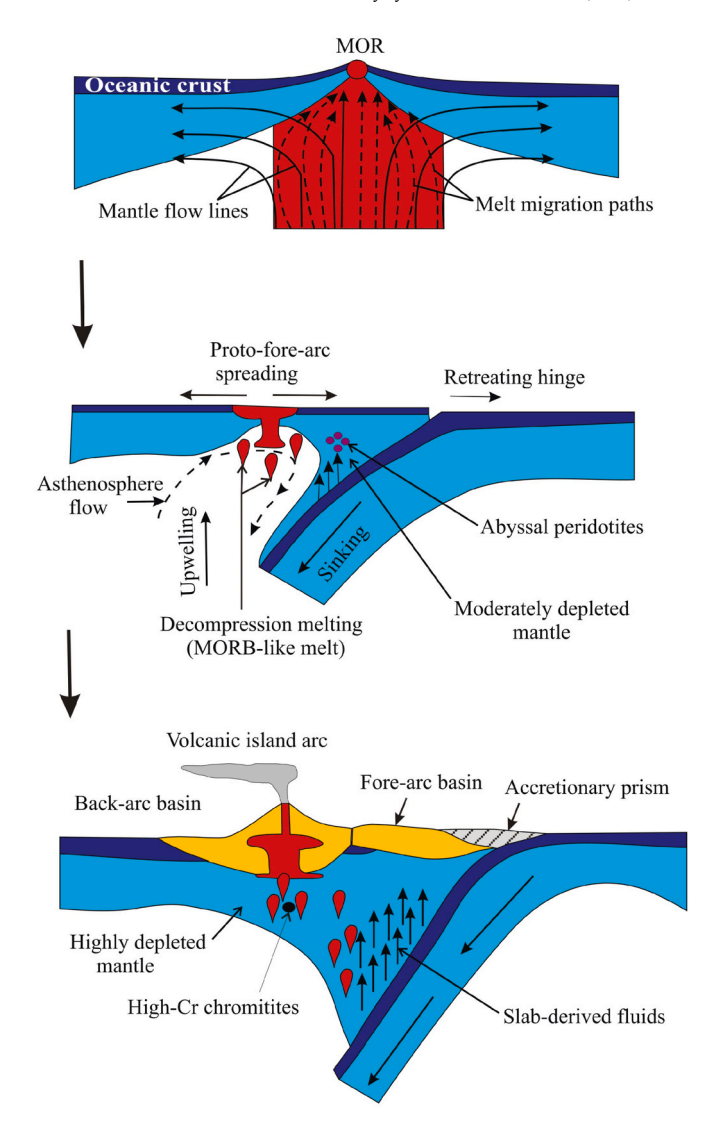


Fig. 9. (a) MgO/SiO $_2$  versus Al $_2$ O $_3$ /SiO $_2$  for the serpentinized ultramafic rocks of the Bir Umq ophiolite; field of fore-arc peridotites after Pearce et al. (2000) and Parkinson and Pearce (1998), depleted mantle and primitive mantle values are from Salters and Stracke (2004) and McDonough and Sun (1995), abyssal peridotites field after Niu (2004), terrestrial array is according to Jagoutz et al. (1979) and Hart and Zindler (1986). (b) CaO vs. Al $_2$ O $_3$  discrimination diagram for serpentinized peridotites (Ishii et al., 1992).

Zoheir and Lehmann, 2011; Azer, 2013; Gahlan et al., 2018; Moussa et al., 2021) and Saudi Arabia (Gahlan et al., 2020b). Zoheir (2011) and Gahlan et al. (2018) obtained quite similar temperatures (~229–340 °C) for chlorite in listvenites in the south Eastern Desert of Egypt. In Saudi Arabia, Gahlan et al. (2020a) obtained slightly lower temperatures (~208–260 °C) for chlorite in Ess listvenites than those in the Eastern Desert of Egypt. The chlorite temperatures of listvenites from the Eastern Desert of Egypt and Saudi Arabia are plainly higher than the inferred maximum temperatures of ~65 °C for listvenite formation proposed by Wilde et al. (2002) or the magnesite clumped isotope temperatures of 65–114 °C for Oman listvenite inferred by Falk and Kelemen (2015). The estimated temperatures for the ANS listvenites are similar to temperatures estimated by numerous authors for other listvenites worldwide (e. g., Buisson and Leblanc, 1987; Spiridonov, 1991; Schandl and Wicks, 1993; Schandl and Gorton, 2012).

## 7.4. Economic potential of Au in the listvenite bodies

The present study indicates that listvenitization concentrates gold in the alteration products to grades that may well reach economic proportions. Sulfides are abundant in the listvenite samples, especially the



**Fig. 10.** Schematic illustration showing the generation of the ANS ophiolites in a fore-arc supra-subduction zone setting.

gold-bearing samples. This indicates that mobilization and transportation of gold in the fluid is associated with complexation with sulfur and that crystallization of solid sulfides provides a host to immobilize and concentrate Au and associated metals (Gahlan et al., 2020a).

Reflected light microscopy and SEM/EDS studies of these samples reveal *in situ* flakes of native gold in silica-carbonate listvenite. However, Au–Pt–Pd alloy is also found in carbonate listvenite. At the microscale, the local host for the observed Au and precious metal alloy flakes is goethite, often extremely enriched in As. This supports the mobilization of Au by oxidizing late fluid infiltration. The current results are consistent with those of other Au-bearing listvenite localities in the Nubian shield (e.g., Zoheir and Lehmann, 2011; Azer, 2013), the Arabian shield (Buisson and Leblanc, 1987; Harbi et al., 2006; Al Jahdali et al., 2003; Al Jahdali, 2004; Gahlan et al., 2020a), and worldwide (e.g., Buisson and LeBlanc, 1985, 1986; Ash and Arksey, 1990; Aydal, 1990; Koç and Kadıolu, 1996; Ucurum and Larson, 1999; Uçurum, 2000; Belogub et al., 2017)

Evidently, the observed concentrations (up to  $3712 \text{ ng g}^{-1}$ ) of Au in mineralized silica-carbonate samples collected in outcrop motivate further exploration of the alteration zones of Bir Umq. Proper evaluation of the potential of the area as an economic gold resource will require collection of boreholes that penetrate the fault planes at depth.

#### 8. Conclusions

- > The Bir Umq ophiolite is situated along the Bir Umq suture zone. It is a dismembered ophiolitic section, tectonically enclosed within or thrust over island arc assemblages. Most of the exposure is mantle section of highly serpentinized ultramafics, with attenuated relics of overlying crustal section of metagabbro, plagiogranite and mélange.
- > The Bir Umq ophiolitic rocks are strongly deformed, metamorphosed, and altered by carbonatization and silicification. Along fault planes and shear zones, the ultramafic rocks are altered into assemblages of talc-carbonate, magnesite and listvenite.
- ➤ Nearly all the primary silicate minerals in the serpentinized ultramafics have been replaced by serpentine minerals, leaving only relics of primary olivine and chromian spinel. The whole-rock chemistry and the abundance of bastite and mesh textures suggest that the peridotite protoliths were mainly harzburgite with minor dunite. The serpentinized peridotites have high Mg#, Ni, Cr, and Co combined with low CaO and Al₂O₃, indicating a highly refractory mantle protolith most consistent with a supra-subduction zone fore-arc setting.
- > Listvenite bodies of various shapes and sizes are developed in the hanging walls of thrust faults within the mantle section. There is an early generation of carbonate listvenite, a later generation of silicacarbonate listvenite, and a final episode of mineralization affecting some silica-carbonate listvenite outcrops. The listvenites formed by replacement of serpentinite protoliths.
- ➤ The first stage of carbonate listvenitization was apparently contemporaneous with serpentinization and emplacement of the mantle section of the Bir Umq ophiolite into oceanic lithosphere. CO₂-bearing fluids were likely derived from the downgoing slab beneath the fore-arc. The second stage of silicification, yielding silica-carbonate listvenite, is associated with ophiolite obduction. Silica and CO₂-bearing fluids were likely released from continental shelf sedimentary sequences in the footwall of the obduction thrust.
- ➤ Listvenitization resulted in a noticeable enrichment in the precious metals, especially gold. This enrichment is most strongly focused in the mineralized silica-carbonate samples, which may have been affected by a third episode of fluid alteration after obduction.

# Declaration of competing interest

The authors declare that they have no known competing financial interests or personal relationships that could have appeared to influence the work reported in this paper.

## Acknowledgements

The authors would like to extend their appreciation and gratitude to the Deanship of Scientific Research, King Saud University for funding and supporting this work through Research Group No. RG-1436-036. Analytical work at the Caltech GPS Division Analytical Facilities is partially supported by NSF Grants EAR-0318518 and DMR-0080065. PDA acknowledges NSF award 1911902. The authors are indebted to the editor (Prof. Mohamed G. Abdelsalam) and highly appreciate thoughtful reviews by Prof. Ghaleb Jarrar and an anonymous reviewer.

## Appendix A. Supplementary data

Supplementary data to this article can be found online at https://doi.org/10.1016/j.jafrearsci.2022.104517.

#### References

Abdel-Karim, A., El-Shafei, S., Azer, M., 2021. The Neoproterozoic ophiolitic ultramafic rocks in Eastern Desert of Egypt: implications for petrogenesis and metasomatic processes. Int. Geol. Rev. 63 (2), 208–232.

- Abuamarah, B.A., 2020. Geochemistry and fore-arc evolution of upper mantle peridotites in the cryogenian Bir Umq ophiolite, arabian shield, Saudi Arabia. Int. Geol. Rev. 62, 630–648.
- Abuamarah, B.A., Asimow, P.D., Azer, M.K., Ghrefat, H., 2020. Suprasubduction-zone origin of the podiform chromitites of the Bir tuluhah ophiolite, Saudi Arabia, during neoproterozoic assembly of the arabian shield. Lithos 360–361, 105439.
- Agar, R.A., Stacey, J.S., Whitehouse, M.J., 1992. Evolution of the Southern Afif Terrane
   a Geochronologic Study. Saudi Arabian Deputy Ministry for Mineral Resource
   Open File Report DGMR-OF-10-15, p. 41.
- Ahmed, A.H., Harbi, H.M., Habtoor, A.M., 2012. Compositional variations and tectonic settings of podiform chromitites and associated ultramafic rocks of the Neoproterozoic ophiolite at Wadi Al Hwanet, northwestern Saudi Arabia. J. Asian Earth Sci. 56, 118–134.
- Ahmed, Z., Hariri, M.M., 2008. Neoproterozoic ophiolites as developed in Saudi Arabia and their oceanic and pericontinental domains. Arabian J. Sci. Eng. 33, 17–54.
- Akbulut, M., Piskin, O., Karayigit, A.I., 2006. The genesis of the carbonatized and silicified ultramafics known as listvenites: a case study from the Mihalıççık region (Eskisehir), NW Turkey. Geol. J. 41 (5), 557–580.
- Al Jahdali, N.S., 2004. Geology of Jabal Ghadarah Area, Bir Tawilah District with Special Emphasis on Listvenite as a Potential Source for Gold in the Kingdom of Saudi Arabia. M.Sc. Thesis. King AbdulAziz University, Jeddah, KSA, p. 197.
- Al Jahdali, N.S., Harbi, H., Eldougdoug, A., 2003. Gold bearing listvenite in jabal Al Ghadarah area, central arabian sheild, kingdom of Saudi Arabia. In: Proceedings of the 8<sup>th</sup> Arab Conference on Mineral Resources, Sanaá. Republic of Yemen, 13-16 October, vol. 1, pp. 26–43.
- Al Shanti, A.M.S., 2009. Geology of the Arabian Shield of Saudi Arabia. Scientific Publications Centre, King Abdulaziz University, Jeddah, KSA.
- Ali, K.A., Azer, M.K., Gahlan, H.A., Wilde, S.A., Samuel, M.D., Stern, R.J., 2010. Age of formation and emplacement of Neoproterozoic ophiolites and related rocks along the Allaqi Suture, south Eastern Desert, Egypt. Gondwana Res. 18, 583–595.
- Al-Rehaili, M.H., 1980. M.Sc. thesis. In: Geology of the Mafic-Ultramafic Complex of Bir Umq Area. King Abdulaziz University, Jiddah, p. 160.
- Al-Rehaili, M.H., Warden, A.J., 1980. Comparison of the Bir Umq and hamdah ultrabasic complexes, Saudi Arabia. Insitute. Appl. Geol. Bulletin. 3 (4), 143–156.
- Arai, S., Kadoshima, K., Morishita, T., 2006. Widespread arc-related melting in the mantle section of the northern Oman ophiolite as inferred from detrital chromian spinels. J. Geol. Soc. Lond. 163, 869–879.
- Ash, C.H., Arksey, R.L., 1990. The Listwanite-Lode Gold Association in British Columbia.

  Geological Survey Branch, Geological Fieldwork 1989, Paper 1990-1, pp. 359–364.

  Avdal D. 1990. Gold-bearing listwaenites in the arac massif kastamonu. Turkey Terra
- Aydal, D., 1990. Gold-bearing listwaenites in the arac massif, kastamonu, Turkey. Terra. Nova 2, 43–52.
- Azer, M.K., Stern, R.J., 2007. Neoproterozoic (835-720 Ma) serpentinites in the Eastern Desert, Egypt: fragments of fore-arc mantle. J. Geol. 115, 457–472.
- Azer, M.K., 2013. Evolution and economic significance of listwaenites associated with Neoproterozoic ophiolites in south Eastern Desert, Egypt. Geol. Acta 11 (1), 113–128.
- Azer, M.K., Asimow, P.D., 2021. Petrogenetic Evolution of the Neoproterozoic Igneous Rocks of Egypt. In the Geology of the Egyptian Nubian Shield. Springer, pp. 343–382. Cham.
- Azer, M.K., Gahlan, H.A., Asimow, P.D., Mubarak, H.S., Al-Kahtany, K.M., 2019. Multiple stages of carbonation and element redistribution during formation of ultramafichosted magnesite in Neoproterozoic ophiolites of the Arabian-Nubian Shield, Egypt. J. Geol. 127 (1), 81–107 ().
- Barnes, S.J., Röeder, P.L., 2001. The range of spinel compositions in terrestrial mafic and ultramafic rocks. J. Petrol. 42, 2279–2302.
- Beinlich, A., Plümper, O., Hövelmann, J., Austrheim, H., Jamtveit, B., 2012. Massive serpentinite carbonation at Linnajavri, N–Norway. Terra. Nova 24 (6), 446–455.
- Belogub, E.V., Melekestseva, I.Y., Novoselov, K.A., Zabotina, M.V., Tret'yakov, G.A., Zaykov, V.V., Yuminov, A.M., 2017. Listvenite-related gold deposits of the South Urals (Russia): a review. Ore Geol. Rev. 85, 247–270.
- Bonatti, E., Michael, P.J., 1989. Mantle peridotites from continental rifts to oceanic basins to subduction zones. Earth Planet Sci. Lett. 91, 297–311.
- Boschi, C., Früh-Green, G.L., Delacour, A., Karson, J.A., Kelley, D.S., 2006. Mass transfer nd fluid flow during detachment faulting and development of an oceanic core complex, Atlantis Massif (MAR 30°N). G-cubed 7, 1.
- Boskabadi, A., Pitcairn, I.K., Broman, C., Boyce, A., Teagle, D.A.H., Cooper, M.J., Azer, M.K., Mohamed, F.H., Stern, R.J., Majka, J., 2017. Carbonate alteration of ophiolitic rocks in the Arabian–Nubian Shield of Egypt: sources and compositions of the carbonating fluid and implications for the formation of Au deposits. Int. Geol. Rev. 59 (4), 391–419.
- Buisson, G., LeBlanc, M., 1985. Gold in carbonatized ultramafic rocks from ophiolite complexes. Econ. Geol. 80, 2028–2029.
- Buisson, G., Leblanc, M., 1986. Gold-bearing listwaenites (carbonatized ultramafic rocks) from ophiolite complexes. In: Gallagher, J.M., Ixer, R.A., Neary, C.R. (Eds.), Metallogeny of Basic and Ultrabasic Rocks. Institution of Mining and Metallurgy, London, pp. 121–132.
- Buisson, G., Leblanc, M., 1987. Gold in mantle peridotites from upper proterozoic ophiolites in Arabia, Mali, and Morocco. Econ. Geol. 82 (8), 2091–2097.
- Coleman, R.G., 1977. Ophiolites. Springer-Verlag, Berlin, p. 229.
- Deer, W.A., Howie, R.A., Zussman, J., 1992. An Introduction to the Rock Forming Minerals, second ed. Longman Scientific and Technical, London, p. 696pp.
- Deschamps, F., Godard, M., Guillot, S., Hattori, K., 2013. Geochemistry of subduction zone serpentinites: a review. Lithos 178, 96–127.
- Dilek, Y., Ahmed, Z., 2003. Proterozoic ophiolites of the Arabian Shield and their significance in Precambrian tectonics. Geol. Soc. 218 (1), 685–700.

- Dunlop, H.M., Kemp, J., Calvez, J.Y., 1986. Geochronology and Isotope Geochemistry of the Bir Umq Mafic-Ultramafic Complex and Arj-Group Volcanic Rocks, Mahd Adh Dhahab Quadrangle, Central Arabian Shield: Saudi Arabian Deputy Ministry for Mineral Resources Open-File Record BRGM-OF-O7-7, p. 38.
- Evans, B.W., 2010. Lizardite Vs. antigorite serpentinite: magnetite, hydrogen, and life (?). Geology 38, 879–882.
- Evensen, N.M., Hamilton, P.J., O' Nions, R.K., 1978. Rare earth abundances in chondritic meteorites. Geochem. Cosmochim. Acta 42 (8), 1199–1212.
- Falk, E.S., Kelemen, P.B., 2015. Geochemistry and petrology of listvenite in the Samail ophiolite, Sultanate of Oman: complete carbonation of peridotite during ophiolite emplacement. Geochem. Cosmochim. Acta 160, 70–90.
- Gahlan, H.A., Azer, M.K., Asimow, P.D., 2018. On the relative timing of listwaenite formation and chromian spinel equilibration in serpentinites. Am. Mineral. 103, 1087–1102.
- Gahlan, H.A., Azer, M.K., Asimow, P.D., Al-Kahtany, K.M., 2020a. Petrogenesis of gold-bearing listvenites from the carbonatized mantle section of the neoproterozoic Ess ophiolite, western arabian shield, Saudi Arabia. Lithos 12, 105679.
- Gahlan, H.A., Azer, M.K., Asimow, P.D., Al-Kahtany, K.M., 2020b. Genesis and geodynamic evolution of serpentinized ultramafics and the associated magnesite deposits, Al-Wask ophiolite, Arabian Shield, Saudi Arabia. Am. J. Sci. 320 (3), 236–279
- Gahlan, H.A., Azer, M.K., Asimow, P.D., Mubarak, H.S., Al-Kahtany, K.M., 2020c. Petrological characteristics of the Neoproterozoic Ess ophiolite mantle section, Arabian Shield, Saudi Arabia: a mineral chemistry perspective. Int. J. Earth Sci. 109, 239–251
- Gahlan, H.A., Azer, M.K., Al-Kahtany, K.M., 2021. Petrogenesis and geodynamic setting of high-Cr chromitites in fore-arc peridotites: a case study from the Halaban ophiolite, Eastern Arabian Shield, Saudi Arabia. Lithos 396–397, 106243.
- Genna, A., Nehlig, P., Le Goff, E., Guerrot, C., Shanti, M., 2002. Proterozoic tectonism of the arabian shield. Precambrian Res. 117 (1–2), 21–40.
- Ghiorso, M.S., Hirschmann, M.M., Reiners, P.W., Kress III, V.C., 2002. The pMELTS: a revision of MELTS for improved calculation of phase relations and major element partitioning related to partial melting of the mantle to 3 GPa. G-cubed 3 (5), 1–35.
- Gillis, K.M., Meyer, P.S., 2001. Metasomatism of oceanic gabbros by late stage melts and hydrothermal fluids: evidence from the Rare Earth element composition of amphiboles. G-cubed 2, 3.
- Habtoor, A.M., Ahmed, A.H., Akizawa, N., Harbi, H., Arai, S., 2017. Chemical homogeneity of high-Cr chromitites as indicator for widespread invasion of boninitic melt in mantle peridotite of Bir Tuluha ophiolite, Northern Arabian Shield, Saudi Arabia. Ore Geol. Rev. 90, 243–259.
- Halls, C., Zhao, R., 1995. Listvenite and related rocks: perspectives on terminology and mineralogy with reference to an occurrence at Cregganbaun, Co. Mayo, Republic of Ireland. Miner. Deposita 30 (3–4), 303–313.
- Hamdy, M.M., Gamal El Dien, H.M., 2017. Nature of serpentinization and carbonation of ophiolitic peridotites (Eastern Desert, Egypt): constrains from stable isotopes and whole rock geochemistry. Arabian J. Geosci. 10 (19), 429.
- Hamdy, M.M., Lebda, E.M., 2007. Metamorphism of ultramafic rocks at gebel arais and gebel malo grim, Eastern Desert, Egypt: mineralogical and O-H stable isotopic constraints. Egypt. J. Geol. 51, 105–124.
- Harbi, H.M., Hassanen, M.A., Eldougdoug, A.A., Sahal, M.S.A., 2003. Geological and Geochemical Studies on Some Gold Occurrences in Zalim Quadrangle, Western Afif Terrane, Arabian Shield, Kingdom of Saudi Arabia. King Abdul Aziz University.
   Research Council p. 69n Project No. 421/203
- Research Council, p. 69p. Project No. 421/203.

  Harbi, H., Eldougdoug, A., Al Jahdali, N.S., 2006. Geology and geochemistry of jabal Ghadarah ophiolitic mélange, zalim quadrangle, Central Saudi Arabia. J. King Abdulaziz University. 17, 117–153.
- Harbi, H., Eldougdoug, A., Madani, A., Ahmed, A., 2011. Listvenite Rocks along Ophiolitic Belts in the Arabian Shield as a Future Potential Source of Gold in Saudi Arabia: with a Special Emphasis on the Application of Remote Sensing and GIS. Final Report (Project No. AT-27-73). King Abdulaziz City for Science and Technology (KACST), Riyadh, Saudi Arabia.
- Hargrove, U.S., Stern, R.J., Kimura, J.I., Manton, W.I., Johnson, P.R., 2006a. How juvenile is the Arabian–Nubian Shield? Evidence from Nd isotopes and pre-Neoproterozoic inherited zircon in the Bi'r Umq suture zone, Saudi Arabia. Earth Planet Sci. Lett. 252, 308–326.
- Hargrove, U.S., Stern, R.J., Griffin, W.R., Johnson, P.R., Abdelsalam, M.G., 2006b. From Island Arc to Craton: Timescales of Crustal Formation along the Neoproterozoic Bi'r Umq Suture Zone, Kingdom of Saudi Arabia. Saudi Geological Survey Technical Report SGS-TR-2006-6, p. 69.
- Hart, S.R., Zindler, A., 1986. In search of a bulk-earth composition. Chem. Geol. 57, 247–267.
- Hinsken, T., Brocker, M., Strauss, H., Bulle, F., 2017. Geochemical, isotopic and geochronological characterization of listvenite from the upper unit on tinos, cyclades, Greece. Lithos 282–283, 281–297.
- Ishii, T., Robinson, P.T., Maekawa, H., Fiske, R., 1992. Petrological studies of peridotites from diapiric Serpentinite Seamounts in the Izu- Ogasawara-Mariana forearc, leg 125. In: Pearce, J., Stokking, L.B., et al. (Eds.), Proceedings of the Ocean Drilling Project, Leg 125, Scientific Results (College Station), pp. 445–485.
- Jagoutz, E., Palme, H., Baddenhausen, H., Blum, K., Cendales, M., Dreibus, G., Spettel, B., Lorenz, V., Vanke, H., 1979. The abundance of major, minor and trace elements in the earth's mantle as derived from primitive ultramafic nodules. Geochem. Cosmochim. Acta 11, 2031–2050.
- Johnson, P.R., 2003. Post-amalgamation basins of the NE Arabian shield and implications for Neoproterozoic III tectonism in the northern East African orogen. Precambrian Res. 123 (2–4), 321–337.

- Johnson, P.R., Woldehaimanot, B., 2003. Development of the arabian-nubian shield: perspectives on accretion and deformation in the northern east african orogen and the assembly of Gondwana. In: Yoshida, M., Dasgupta, S., Windley, B. (Eds.), Proterozoic East Gondwana: Supercontinent Assembly and Breakup, vol. 206. Geological Society of London Special Publications, pp. 289–325.
- Kelemen, P.B., Hirth, G., Shimizu, N., Spiegelman, M., Dick, H.J.B., 1997. A review of melt migration processes in the adiabatically upwelling mantle beneath oceanic spreading ridges. Philos. Trans. R. Soc. London, Ser. A 355, 283–318.
- Kelemen, P.B., Matter, J., Streit, E.E., Rudge, J.F., Curry, W.B., Blusztajn, J., 2011. Rates and mechanisms of mineral carbonation in peridoitte: natural processes and recipes for enhanced, in situ CO2 capture and storage. Annu. Rev. Earth Planet Sci. 39, 545–576
- Kemp, J., Gros, Y., Prian, J.P., 1982. Geologic Map of the Mahd AHD Dhahab Quadrangle Sheet 23 E, Kingdom of Saudi Arabia.
- Koç, S., Kadıoğlu, Y.K., 1996. Mineralogy, geochemistry and precious metal content of Karacakaya (Yunusemre-Eskisehir) listwaenites. Ofioliti 21, 125–130.
- Kröner, A., Linnebacher, P., Stern, R.J., Reischmann, T., Manton, W.I., Hussein, I.M., 1991. Evolution of Pan-African island arc assemblages in the southern Red Sea Hills, Sudan and in southwestern Arabia as exemplified by geochemistry and geochronology. Precambrian Res. 53, 99–118.
- Lebda, E.M., 1995. Petrology and Mineral Chemistry of Serpentinite Rocks of the Gogolow-Jordanow Massif, SW Poland. Ph.D. Thesis. Wrocław University, Poland, p. 189.
- Likhoidov, G.G., Plyusnina, L.P., Shcheka, Z.A., 2007. The behavior of gold during listvenitization: experimental and theoretical simulation. Dokl. Earth Sci. 415 (5), 723–726
- McDonough, W.F., Sun, S.S., 1995. Composition of the earth. Chem. Geol. 120, 223–253.
   McElduff, B., Stumpfl, E.F., 1991. The chromite deposits of the Troodos complex, Cyprusevidence for the role of a fluid phase accompanying chromite formation. Miner. Deposita 26 (4), 307–318 ().
- Meert, J.G., 2003. A synopsis of events related to the assembly of eastern Gondwana. Tectonophysics 362, 1–40.
- Mellini, M., Rumori, C., Viti, C., 2005. Hydrothermally reset magmatic spinels in retrograde serpentinites: formation of "ferritchromit" rims and chlorite aureoles. Contrib. Mineral. Petrol. 149, 266–275.
- Moussa, H.E., Azer, M.K., Abou El Maaty, M.A., Maurice, A.E., Yanni, N.N., Akarish, A.I., Elnazer, A.A., Elsagheer, M.A., 2021. Carbonation of Neoproterozoic mantle section and formation of gold-bearing listvenite in the Northern Nubian Shield. Lithos 406 (407), 106525.
- Mubarak, H.S., Azer, M.K., Surour, A.A., Moussa, H.E., Asimow, P.D., Kabesh, M., 2020.Mineralogical and geochemical study of rodingites and associated serpentinized peridotite, Eastern Desert of Egypt, Arabian-Nubian Shield. Lithos 374–375, 105720.
- Nehlig, P., Genna, A., Asfirane, F., 2002. A review of the pan-african evolution of the arabian shield. GeoArabia 7, 103–124.
- Newton, R.C., Stern, R.J., 1990. A Late Precambrian CO2 "Event". Geological Society of America, Dallas, p. 190.
- Niu, Y., 2004. Bulk-rock major and trace element compositions of abyssal peridotites: implications for mantle melting, melt extraction and post-melting processes beneath mid-ocean ridges. J. Petrol. 45, 2423–2458.
- Olivier, N., Boyet, M., 2006. Rare earth and trace elements of microbialites in Upper Jurassic coral-and sponge-microbialite reefs. Chem. Geol. 230, 105–123.
- Pallister, J.S., Stacey, J.S., Fischer, L.B., Premo, W.R., 1988. Precambrian ophiolites of Arabia: geologic settings, U-BP geochronology, BP-isotope characteristics, and implications for continental accretion. Precambrian Res. 38, 1–54.
- Parkinson, I.J., Pearce, J.A., 1998. Peridotites from the Izu-Bonin-Mariana forearc (ODP Leg 125): evidence for mantle melting and melt-mantle interaction in a suprasubduction zone setting. J. Petrol. 39, 1577–1618.
- Paulick, H., Bach, W., Godard, M., De Hoog, J.C.M., Suhr, G., Harvey, J., 2006. Geochemistry of abyssal peridotites (Mid-Atlantic Ridge, 15°20\ N, ODP Leg 209): implications for fluid/rock interaction in slow spreading environments. Chem. Geol. 234, 179–210.
- Pearce, J.A., Barker, P.F., Edwards, S.J., Parkinson, I.J., Leat, P.T., 2000. Geochemistry and tectonic significance of peridotites from the South Sandwich arc-basin system, South Atlantic. Contrib. Mineral. Petrol. 139, 36–53.
- Pirouei, M., Kolo, K., Kalaitzidis, S.P., 2020. Hydrothermal listvenitization and associated mineralizations in Zagros Ophiolites: implications for mineral exploration in Iraqi Kurdistan. J. Geochem. Explor. 208, 106–404.
- Plissart, G., Féménias, O., Māruntiu, M., Diot, H., Demaiffe, D., 2009. Mineralogy and geothermometry of gabbro-derived listvenites in the Tisovita–Iuti ophiolite, Southwestern Romania. Can. Mineral. 47 (1), 81–105.
- Power, I.M., Harrison, A.L., Dipple, G.M., Wilson, S.A., Kelemen, P.B., Hitch, M., Southam, G., 2013. Carbon mineralization: from natural analogues to engineered systems. Rev. Mineral. Geochem. 77 (1), 305–360.
- Ramadan, T.M., Sadek, M.F., Abu El Leil, I., Salem, S.M., 2005. Um El touyur El fuqani gold mineralization, south Eastern Desert, Egypt: using landsat ETM+ imagery. Ann. Geol. Surv. Egypt 28, 263–281.
- Salters, V.J., Stracke, A., 2004. Composition of the depleted mantle. G-cubed 5 (5). Schandl, E.S., Gorton, M.P., 2012. Hydrothermal alteration and  ${\rm CO_2}$  metasomatism (natural carbon sequestration) of komatiites in the south-western Abitibi greenstone belt. Can. Mineral. 50, 129–146.
- Schandl, E.S., Wicks, F.J., 1993. Carbonate and associated alteration of ultramafic and rhyolitic rocks at the hemingway property, kidd creek volcanic complex, timmins, ontario. Econ. Geol. 88, 1615–1635.
- Shahien, M.G., Azer, M.K., Asimow, P.D., 2021. Neoproterozoic ophiolites of the arabiannubian shield. In: Hamimi, Z., Fowler, A.-R., Liegeois, J.-P., Collins, A.,

- Abdelsalam, M., Abd El-Wahed, M. (Eds.), The Geology of the Arabian-Nubian Shield. Springer, ISBN 978-3-030-72994-3.
- Spiridonov, E.M., 1991. Listvenites and zodites. Int. Geol. Rev. 33, 397–407.
- Suita, M., Strieder, A., 1996. Cr-spinels from Brazilian mafic-ultramafic complexes: metamorphic modifications. Int. Geol. Rev. 38, 245–267.
- Thalhammer, O.A.R., Prochaska, W., Mühlhans, H.W., 1990. Solid inclusions in chromespinels and platinum group element concentrations from the Hochgrössen and Kraubath Itramafic massifs (Austria). Contrib. Mineral. Petrol. 105 (1), 66–80 ().
- Uçurum, A., 2000. Listwaenites in Turkey: perspectives on formation and precious metal concentration with reference to occurrences in east-central Anatolia. Ofioliti 25 (1), 15–29.
- Ucurum, A., Larson, L.T., 1999. Geology, base-precious metal concentration and genesis of the silica-carbonate alteration (listvenites) from late cretaceous ophiolitic mélanges at central east Turkey. Chem. Erde 59 (2), 77–104.
- Van Noort, R., Spiers, C.J., Drury, M.R., Kandianis, M.T., 2013. Peridotite dissolution and carbonation rates at fracture surfaces under conditions relevant for in situ mineralization of CO<sub>2</sub>. Geochem. Cosmochim. Acta 106, 1–24.
- Wilde, A., Simpson, L., Hanna, S., 2002. Preliminary study of Cenozoic alteration and platinum deposition in the Oman ophiolite. J. Virtual Explor. 6, 7–13.
- Whitehouse, M.J., Stoeser, D., Stacey, J.S., 2001. The khida terrane geochronological and isotopic evidence for paleoproterozoic and archean crust in the eastern arabian shield of Saudi Arabia. Gondwana Res. 4, 200–202.
- Zoheir, B., 2011. Transpressional zones in ophiolitic mélange terranes: potential exploration targets for gold in the South Eastern Desert, Egypt. J. Geochem. Explor. 111, 23–38.
- Zoheir, B.A., Lehmann, B., 2011. Listvenite-lode association at the barramiya gold mine, Eastern Desert, Egypt. Ore Geol. Rev. 39, 101–115.